U.PORTO

FEUP FACULDADE DE ENGENHARIA
UNIVERSIDADE DO PORTO

SCOUR AT OFFSHORE WIND STRUCTURES IN COMPLEX SOILS

ANA MARGARIDA MARTINS CHAVES

Dissertation submitted for the degree on

MASTER IN ENVIRONMENTAL ENGINEERING

Supervisor: Professor Tiago João Fazeres Ferradosa

Co-Supervisor: Professor Paulo Jorge Rosa Santos

Co-Supervisor: Professor Elsa Maria da Silva Carvalho

July, 2024

Aos meus pais

“Tudo é ousado para quem a nada se atreve.”

Fernando Pessoa

ACKNOWLEGDMENTS

First of all, I would like to thank my supervisor Professor Doctor Tiago João Fazeres Ferradosa and my co-supervisors Professor Doctor Paulo Jorge Rosa Santos and Professor Doctor Elsa Maria da Silva Carvalho for the opportunity to carry out this dissertation. A special thanks to Professor Doctor Tiago Ferradosa for the teaching, the working conditions, his motivation and, above all, his contagious good mood.

To Eng. Filipe Miranda, because without his help this work would not have gone as well as it did. I would like to thank for his tireless support every day every hour, for always reminding me the Murphy's Law, his motivation and for passing on all the teachings necessary for this dissertation.

To Eng. Tomás Cabral and Eng. João Chambel for always being willing to help me with any problem I encountered in the laboratory. Thank you for your constant support. I would also like to thank everyone I met at SHRHA for welcoming me and treating me so well. To Eng. Patricia for helping me at the LEMC with the granulometric analysis of the sands and for the care she showed so that I understood everything I was doing. A huge thank you to Sr. Miguel for his constant support, kindness, help at any time, concern, long conversations and his intention to do everything he could to ensure that my work went well.

To my friends from Chaves, my hometown, thank you for so many years of strong friendship, for always supporting me and for the patience to put up with me. I have to highlight one in particular, Benny, because this semester you were a precious help, you put up with me in the worst moments, you always showed support so that this work went smoothly and above all for the affection with which you never failed me.

To my Rattatitãns, my friends from FEUP, those who have made these five years fly by. Always with me when I laugh or cry. For all the moments thank you for being there, you are my friends for life.

To André for supporting me during the last few months of this work, for your constant patience, for being annoying but managing to bring me calm every day. Thank you for believing in me

To my brothers Zé and Chico thank you for the last 23 years, for all the strange forms of love, affection, resilience and hard work that you have shown me. To Joana and Tamila, for all the kindness and support you gave me. To António and Manuel for simply existing and for all the joy they bring me.

By last but not least, to my parents, my greatest support throughout my life, thank you for the love and everything they've done and faced so that I could get here. Dad, for all the laughs, jokes and kindness you showed me every day. Mom, my biggest hero, thank you for showing me what it means to be resilient and showing that we are all capable of achieving what we want, we just have to take the risk

This work was financially supported by Project PTDC-ECI-EGC-5177-2020 (POSEIDON project), funded by national funds through FCT- Portuguese Foundation for Science and Technology.

ABSTRACT

The transition to renewable energy is essential for addressing climate change and ensuring sustainable energy sources for the future. Offshore wind energy plays a crucial role in this transition, offering a vast potential for clean energy generation. However, the stability and longevity of these structures are challenged by the scour phenomenon around their foundations. Fully understanding the mechanisms that influence scour is paramount for an effective design and maintenance of offshore wind turbines.

Despite all the existing research, there are still literature gaps regarding scour around offshore foundations, particularly the development of scour in complex seabed soils. The present research addresses this gap by exploring how different sediment types and their organization by layers impact the scour process. To achieve this, a series of controlled physical modelling experiments on 1:100 Froude modeling scale were performed in the flume of the Hydraulics Laboratory of the Faculty of Engineering of the University of Porto (FEUP). Five scour tests on a monopile foundation under currents only were carried out, an initial one with a single layer of fine sand, and four tests with a soil composed of two layers of sediment. The sediments used ranged from narrow to wide graded, and a grain size ranging from 0.250-0.500 mm.

The results showed the influence of the uniformity coefficient and grain size in the scour depth of layered tests. They also allowed to confirm that when velocity used in the experimental studies is not critical for any of the sand used, in the layered tests, the scour depth is lower when coarse sand is the top layer.

KEYWORDS: Layered sands, Monopile, Offshore wind turbine, Physical Modeling, Scour

RESUMO

A transição para as energias renováveis é essencial para enfrentar as alterações climáticas e garantir fontes de energia sustentáveis para o futuro. A energia eólica offshore desempenha um papel crucial nesta transição, oferecendo um vasto potencial para a produção de energia limpa. No entanto, a estabilidade e a longevidade destas estruturas são postas em causa pelo fenómeno da erosão em torno das suas fundações. Compreender plenamente os mecanismos que influenciam a erosão é fundamental para uma criação e manutenção eficazes das turbinas eólicas offshore.

Apesar de toda a investigação existente, existem ainda lacunas na literatura no que respeita à erosão em torno das fundações offshore, em particular o desenvolvimento da erosão em solos complexos do fundo do mar. A presente dissertação aborda esta lacuna, explorando a forma como diferentes tipos de sedimentos e a sua organização por camadas afetam o processo de erosão. Para tal, foi realizado no canal do Laboratório de Hidráulica da Faculdade de Engenharia da Universidade do Porto (FEUP) um estudo físico à escala de geométrica 1:100 seguindo a semelhança de Froude. Foram realizados cinco ensaios de erosão numa fundação do tipo monopilar apenas sob correntes, um inicial com uma única camada de areia fina, e quatro ensaios com um solo composto por duas camadas de sedimentos. Os sedimentos utilizados variavam de finos a grossos, com uma granulometria de 0.250-0.500 mm.

Os resultados mostraram a influência do coeficiente de uniformidade e da granulometria dos sedimentos na profundidade da fossa de erosão em ensaios por camadas. Permitiram também saber que, quando a velocidade utilizada nos estudos experimentais não é crítica para nenhuma das areias utilizadas, nos ensaios em camadas, a profundidade de erosão é menor quando a areia grossa está na camada superior.

PALAVRAS-CHAVES: Areia por camadas, Erosão, Modelação Física, Monopilar, Turbina Eólica Offshore

TABLE OF CONTENTS

FIGURES INDEX

TABLES INDEX

NOMENCLATURE

A^*	$[m^2]$	Projected area of the grain on the horizontal plane
D^*	$[-]$	Dimensionless grain size
d_{50}	$[m]$	Mean diameter of bed sediments
$d_{cr,under}$	$[m]$	Particle size of the underlaying layer and erosion will not occur when the particles are larger than this critical value
d_{over}	$[m]$	Particle size for overlying layer
$d_{over}{}'$	$[m]$	Particle size of the overlaying layer, entirely eroded
D_p	$[m]$	Pile diameter
d_{under}	$[m]$	Particle size for underlying layer
d_x	$[m]$	Diameter of sediment grain
f_c	$[-]$	Current friction
F_D	$[N]$	Horizontal drag force
F_L	$[N]$	Vertical lift force
H_r	$[m]$	Ripple's height
K_d	$[-]$	Flow depth factor
K_D	$[-]$	Sand's particles dimensions factor
K_h	$[-]$	Factor that represents the effects of the pile dimensions and water depth
K_I	$[-]$	Factor used to represent the flow intensity
k_s	$[m]$	Bottom roughness
K_s	$[-]$	Shape factor
K_s	$[-]$	Shape factor for uniform piles
K_{si}	$[-]$	Pile size factor
K_t	$[-]$	Time's influence in the scour hole factor
K_α	$[-]$	Pile alignment factor
K_α	$[-]$	Influence of the attack angle to the pile factor
K_θ	$[-]$	Flow angle factor
K_σ	$[-]$	Grain size distribution factor
r_d	$[-]$	Particle size ratio
Re^*	$[-]$	Grain Reynolds number
S_e	$[m]$	Equilibrium scour depth
t_e	$[s]$	Equilibrium time scale
u_*	$[m/s]$	Friction Velocity
U_c	$[m/s]$	Depth average flow velocity

U_{cr}	$[m/s]$	Critical velocity
z_0	$[m]$	Bed roughness length
α_{down}	$[°]$	Downstream scour slope
α_{up}	$[°]$	Upstream scour slope
θ_{cr}	$[-]$	Critical Shields parameter
ρ_s	$[\mathrm{kg/m^3}]$	Sediment density
ρ_s	$[\mathrm{kg/m^3}]$	Density of particle
σ_{D}	$[-]$	Uniformity coefficient
σ_s	$[-]$	Standard deviation of scour depth
$\tau_{\propto}$	$[N/m^2]$	Undisturbed bed shear-stress
τ_0	$[N/m^2]$	Bed Shear-Stress
$\tau_{b,c}$	$[N/m^2]$	Current induced Bed Shear-Stress
τ_b	$[N/m^2]$	Bottom bed shear-stress
τ_{cr}	$[N/m^2]$	Critical bed shear-stress
$\emptyset$	$[-]$	Pile shape factor
C	$[\sqrt{m}/s]$	Chèzy coefficient
d	$[m]$	Water depth
e	$[-]$	Neper's number
g	$[m/s^2]$	Gravitational acceleration
k	$[-]$	Von Karman constant
Re	$[-]$	Reynolds Number
S	$[m]$	Scour depth
t	$[s]$	Time
T	$[s]$	Time of the equilibrium scour depth
U	$[m/s]$	Flow velocity
v	$[m^2/s]$	Kinematic viscosity of water
W	$[m]$	Total scour extent
W	$[m]$	Pile width
z	$[m]$	Vertical distance
α	$[-]$	Amplification factor
θ	$[-]$	Shields Parameter

μ	$[N.s/m^2]$	Dynamic Viscosity
ρ	$[\mathrm{kg/m^3}]$	Density of Water

ABBREVIATIONS

ADV	Acoustic Doppler Velocimeter
EU	European Union
FEUP	Faculty of Engineering of the University of Porto
LCoE	Levelized Cost of Energy
LEMC	Construction Materials Testing Laboratory
PVC	Polyvinyl Chloride
SDG	Sustainable Development Goal
SHRHA	Hydraulics, Water Resources and Environment Division

1 INTRODUCTION

1.1 PRESENTATION

In the last decade, due to advances in wind energy conversion technologies, the global wind energy market has quadrupled and wind energy has proven to be one of the most cost-effective and robust power sources worldwide. It helps combat climate change by reducing fossil fuel consumption for electricity production, which will lead to lower greenhouse gas emissions and less air pollution, thus contributing to a more sustainable energy mix (IRENA 2023).

Europe is the leader in offshore wind and is home to one of the largest operational wind farms for both bottom-fixed and floating foundation technologies (WindEurope 2022). In 2023, in Europe it was installed 18.3 GW of new wind power capacity. The EU-27 installed 16.2 GW of this, a record amount but only half of what it should be building to meet its 2030 climate and energy targets. Europe is expected to install 260 GW of new wind power capacity over 2024-2030. To meet its 2030 climate and energy targets the EU now needs to install 33 GW per year (WindEurope 2023)

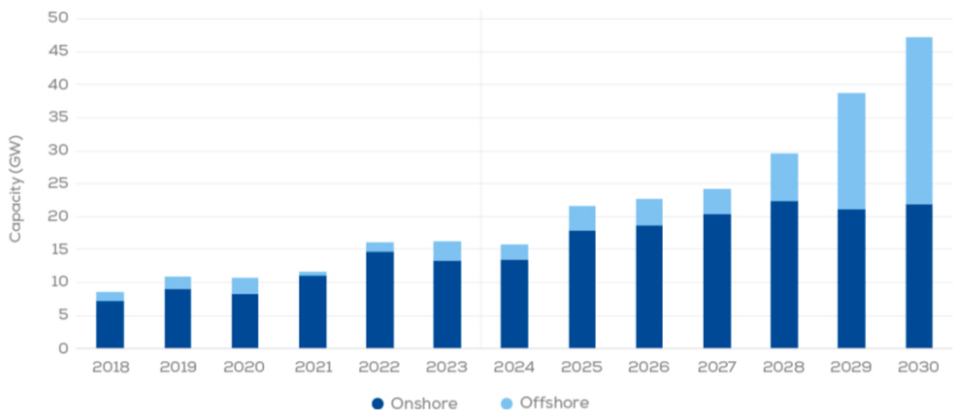

Figure 1. 2024-2030 annual Onshore and offshore wind power capacity installed in Europe (WindEurope 2023).

Wind velocity is higher and more consistent at offshore locations than onshore ones. More importantly, offshore wind energy is known to be characterized by higher power density, and superior capacity factor compared to onshore wind energy. Meanwhile, offshore power installations have shown promising growth over the past few years; and more significant progress in offshore wind technology are expected to be subsequently made with enhancements of research models and engineering designs. On the other hand, one of the main challenging drawbacks that is associated with offshore wind power plants is its high levelized cost of energy (LcOE) (Desalegn, Gebeyehu et al. 2023). Previous studies indicated that the LcOE for offshore systems may be reasonably falling as further future advancements could possibly take place in offshore wind-based research studies and technologies (Desalegn, Gebeyehu et al. 2023).. By 2050 the LcOE wind would be competitive, reaching lower fossil fuel ranges (IRENA 2019), as it can be seen in the Figure 2.

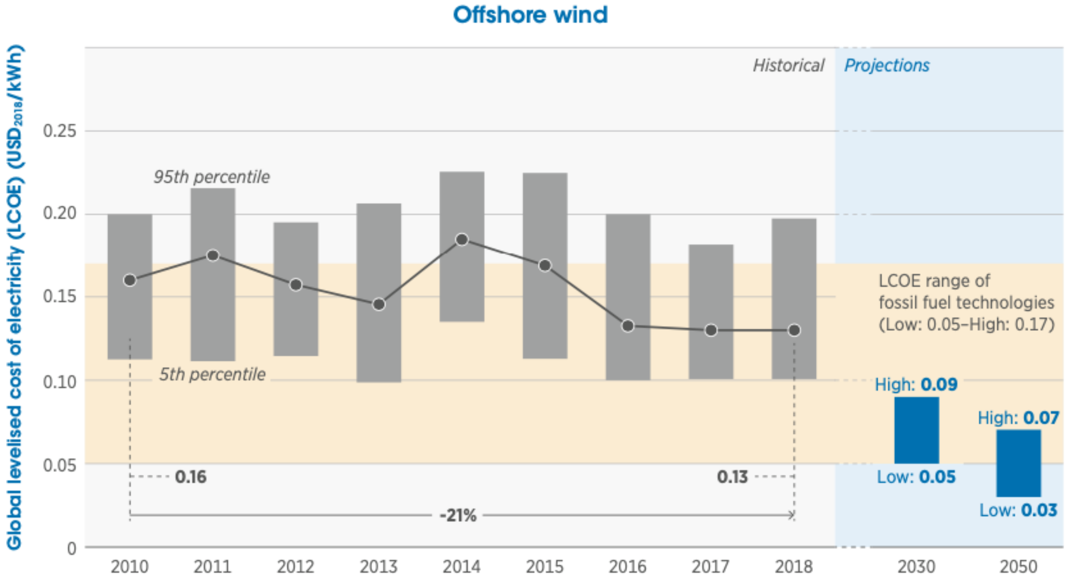

Figure 2. Global levelized cost of energy for offshore wind energy (IRENA 2019)

Offshore wind turbine foundations represent costs around 30% of the overall investment of an offshore windfarm (Matutano 2013). Monopiles remain the most common and cost-effective choice for offshore wind foundations at the moment (Engineering 2023). However, the harsh marine environment presents significant challenges to the durability and efficiency of offshore wind structures. Among these challenges, scour stands out as a critical concern. The decommission of two monopiles at the Robin Rigg wind farm after only six years of operation due to unexpected levels of scour demonstrates the hazard that an active marine environment poses to offshore wind turbines (Menéndez-Vicente, López-Querol et al. 2023). Addressing scour is therefore paramount in ensuring the long-term viability and safety of offshore wind foundations.

1.2. CONTEXT AND OBJECTIVES

The bulk of research concerning scour around offshore wind turbine foundations predominantly focuses on simple soils, leaving a noticeable gap in understanding this phenomenon in complex soils. While studies on simple soils provide valuable insights into the scour process, the diverse and often challenging conditions present in complex soil substrates demand closer attention. The objective of the present research is to study the scour phenomenon on monopiles founded on soils of two different sand layers. The marine soils on which wind structures are founded are often structured by layers of sediments with different characteristics. Addressing this gap by understanding the scour in layered sand substrates will not only enhance the accuracy of predictive models but also contribute significantly to the design and maintenance of offshore turbine foundations, ensuring their long-term stability and performance in varying soil conditions.

This dissertation adds to the body of knowledge on scour processes, particularly in complex soil environments, providing valuable insights for researchers, engineers, and policymakers involved in offshore wind energy development. By advancing scientific understanding and sharing research findings, this work contributes to the continuous improvement of design standards, regulatory frameworks, and industry practices, benefiting the offshore wind industry worldwide.

In this context, this dissertation seeks to understand the phenomenon of scour in complex soils, using reduced scale physical models that are tested in the Hydraulics Laboratory of the Department of Civil Engineering of FEUP.

The main objective is to find the answer to what the primary factors are influencing scour development around offshore wind foundations, and how they change based on the sediments that are being used and their respective layering.

1.3. THESIS ORGANIZATION

The present dissertation is divided in five chapters where the work that was done is described.

In Chapter 1 a brief introduction to the wind energy sector is given, why it is important to study the scour and the main objectives and context of the dissertation.

Chapter 2 presents the basic concepts of scour phenomenon. Here are also presented all the parameters that can influence the scour and a review of previous works that were already done.

Chapter 3 is focused on description of the experimental set-up of the Hydraulic Laboratory, methodologies and equipment used

Chapter 4 is reserved for the presentation and discussions of the final results obtained in the scour tests

Chapter 5 provides the main conclusions that can be drawn from the study carried out. Future works that can be done are also highlighted

The final chapter 6 of the Sustainable Development Goals Alignment presents how the work done in this dissertation is relevant to the achievement of the targets marked by SDG 17.

2 SCOUR PHENOMENON

2.1. FLUID-SOIL-STRUCTURE INTERACTION

Scour is both a hydrodynamic process linked to the seabed sediment motion due to the flow of water around a structure, and a geotechnical process, as it relates to the reduction in ground level around the foundation. The influence of the structure on the flow conditions results in increased erosive capacity in its vicinity. Over time a scour hole can form, which may be large enough to affect the structure's stability (Porter, Harris et al. 2013). A scour hole can be seen in Figure 3.

When the bed sheer stress generated by the friction of the wave flow on the seabed surface surpasses the critical shear stress the particles stars to roll over. The shear stress increases even further, making the particle reach the suspended load layer. The particles remains in suspension as long as the frictional velocity of the particle is bigger than the fall velocity (Collins 2017).

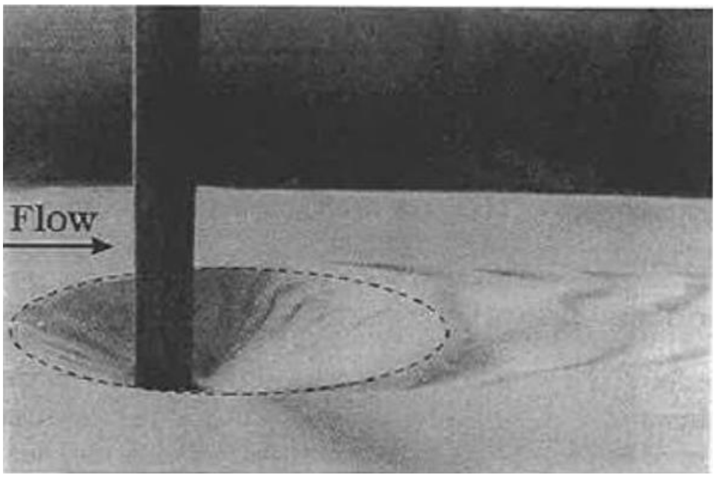

Figure 3. Typical scour hole (Ferradosa 2011)

Many of the scour inducing effects on the seabed around offshore foundations are due to changes in flow patterns resulting from soil-fluid-structure interaction. The monopile offshore wind turbine can be considered as a cylindrical pile. The changes in flow and the respective flow patterns induced by these vertical piles have been studied over the years. When a vertical pile is placed on a seabed, the flow forms the following patterns:

- The downflow;
- The horseshoe vortex;

- The lee-wake vortices;
- The streamlines are contracted at the side edges of the pile.

A sketch of the flow-structure interaction for a vertical cylinder can be seen in Figure 4.

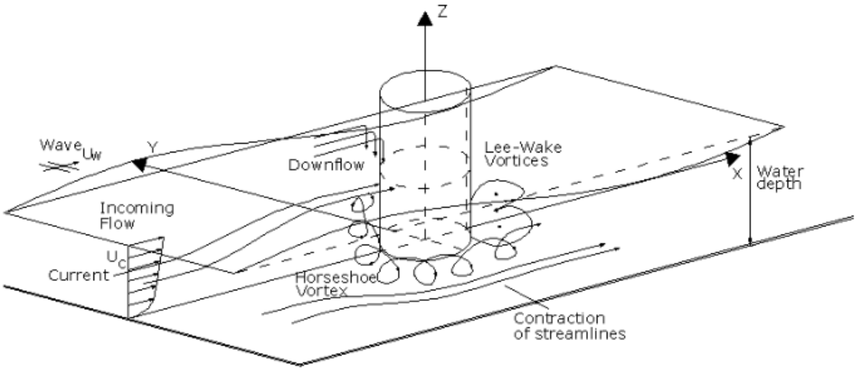

Figure 4. Sketch of the flow-structure interaction for a vertical cylinder (DeVos 2008)

The downflow originates as the flow comes to rest at the front of the pile. Since the velocity decreases from the surface downwards, the stagnation pressure also decreases from the surface down, creating a downward pressure gradient (DeVos 2008).

The horseshoe vortex is the most dominant flow pattern and an important mechanism leading to the scouring of sediment from the base of a vertical cylinder (Whitehouse 1998). The incoming flow rotation creates the horseshoe vortex. This rotation leads to a three-dimensional separation in the bed's boundary layer upstream of the pile, caused by the adverse pressure gradient generated by the structure's presence. The separated boundary later forms a spiral vortex (horseshoe vortex) around the structure and then trails off downstream (DeVos 2008) which can be seen in Figure 5.

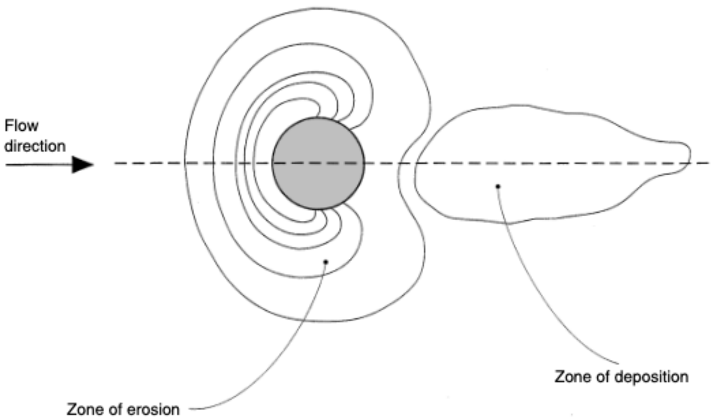

Figure 5. Scour pattern for a vertical cylinder in a steady current (Whitehouse 1998).

The lee-wake vortices are a flow pattern and a scour inducing mechanism generated on the downstream side of the monopile, due to the separation of the flow. These vortices increase the turbulence levels, due to the flow velocity variation, increasing the bed shear stress on the downstream, arising from the pile edges (Chambel 2019). This will lead to scour at the downstream side, and respective sediment transport, until its deposition, away from the structure, when the sheer stress is no longer enough to cause movement (Ferradosa 2018). In case of a steady current, the pile Reynolds number determines the lee-wake vortex flow. The flow changes strongly when the pile Reynolds number increases (DeVos 2008).

The contraction of the streamlines is caused by the separation and bending of the flow around the monopile. As the flow meets the pile on the upstream side, it first slows down before accelerating again around the edges to the downstream side. This process increases shear stress and causes scour near the monopile edges (Sumer and Fredsøe 1997).

Understanding and defining the scour phenomena, along with all associated variables, is essential. This chapter will cover the fundamental concepts related to this topic, providing a foundation for the development of subsequent chapters.

2.2. BED SHEAR-STRESS

The effects of the hydrodynamic forcing agents (currents and waves) on the sediment dynamics take place primarily through the friction they exert on the seabed. This is expressed in terms of the bed shear-stress, which is the frictional force exerted by the flow per unit area of bed (Soulsby 1997).

The bed shear-stress, τ_0, which has units of force per unit area(Nm^{-2} in SI units), can also be written in units of velocity (ms^{-1} in SI units) as the friction velocity (or shear velocity),u_*, which is defined through the relationship (Soulsby 1997):

$$\tau_0 = \rho u_*^2 \tag{1}$$

$$u_* = \left(\frac{\tau_0}{\rho}\right)^{\frac{1}{2}} \tag{2}$$

being ρ the density of the water. A dimensionless form of bed shear-stress, parameter, θ, is represented by the following equation:

$$\theta = \frac{\tau_0}{g(\rho_s - \rho)d} \tag{3}$$

where g is the acceleration due to gravity; ρ the water density; $\rho_s$the density of the sediment and d is the diameter of sediment grains (Soulsby 1997).

2.2.1 BED SHEAR STRESS- CURRENTS

The environment to which an offshore wind structure is exposed to is a very important factor that affects the scour process. The North Sea, where the majority of wind structures are installed, is mostly shallow and rather flat, with an average depth of 80 m (Vindenesa, Orvika et al. 2018). According to Soulsby

(1997) in marine environment currents can be created by tidal motions, wind-stress, atmospheric pressure gradients, wave induced forces, large-scale quasy-steady water surface slopes and horizontal gradients linked to the oceanic circulations. A map of the currents is presented in Figure 6.

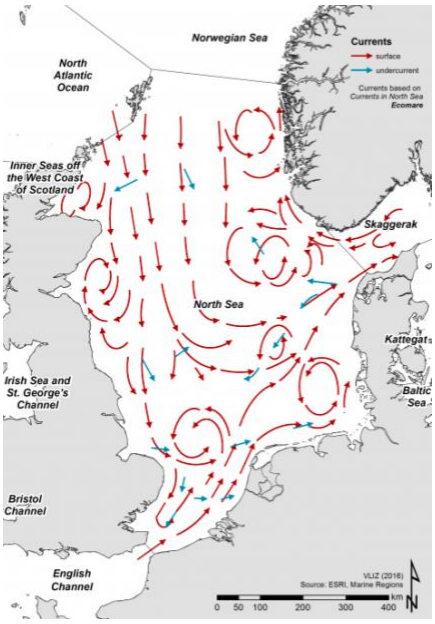

3

Figure 6. Currents in the North Sea (Adapted from (Hauwere 2016)

In the study of Melville (2008) was reported that the equilibrium scour depth increases almost linearly with flow velocity through the clear water regime. If the flow velocity is to low, scour phenomenon will not happen because the shear stress at the structure will not be higher than the critical value. It can be concluded that the depth-averaged flow velocity (U_c), as the current direction and the velocity profiles are the flow characteristics that have the most influence. The bed shear stress that is induced by currents, $\tau_{b,c}$ ($N/\,m^2$), can be calculated by the following equation:

$$\tau_{b,c} = \frac{1}{2}\rho f_c U_c^2 \tag{3}$$

Where f_c represents the current friction factor and U_c the depth-averaged current velocity (Soulsby 1997). According to Liu (2001)the current friction factor, f_c, can be calculated by:

$$f_c = \frac{2g}{C^2} = \frac{2g}{\left(\frac{\sqrt{g}}{k}\ln\left(\frac{d}{z_0 \cdot e}\right)\right)^2} = \begin{cases} \frac{0.06}{\left(\log\left(\frac{12d}{3.3 \cdot \frac{\nu}{u_*}}\right)\right)^2}, & Smooth\ flow: \frac{u_* k_s}{\nu} \leq 5 \\ \frac{0.06}{\left(\log\left(\frac{12d}{k_s}\right)\right)^2}, & Rough\ flow: \frac{u_* k_s}{\nu} \geq 70 \end{cases} \tag{4}$$

In Eq.(4) C is the Chèzy coefficient ($m^{1/2}/s$), k is the Von Karman constant, equal to 0.4, e is the Nepper's number, v is the water kinematic viscosity and z_0 is the roughness length.

Smooth and rough flows are two types of turbulent flow regimes, as shown in Eq.(4) (Chambel 2019). There are two major flow regimes:

- Laminar flow;
- Turbulent flow;

Between both of these flows there is an unstable zone that corresponds to the transition regime. The limits of these regimes can be estimated using the Reynolds Number (Re):

$$Re = \frac{\rho D_p U}{\mu} = \frac{D_p U}{v} \tag{5}$$

Where $U(m/s)$ is the flow velocity, ρ the fluid density (kg/m^3), D_p the pile diameter (m), μ the dynamic viscosity (N.s/m^2) and v the kinematic viscosity (m^2/s).

In the laminar flow (Re<2000), the fluid presents regular trajectories, the fluid particles do not cross each other, the velocity variations are extremely slow in time - or almost nonexistent - and the flow is dominated by viscosity effects, not being affected by the characteristics of the surface of the rigid layer (Webber 1971). In the turbulent flow (Re>4000), the fluid particles have abrupt variations in space and time, the velocity field is also variable in space and time and the regime is separated from the boundary surface by a thin layer in which the flow presents laminar behavior (the so-called laminar boundary sub-layer).

In smooth flow conditions, the surface roughness of the bed is minimal, and it doesn't significantly alter the velocity distribution because the roughness elements remain within the thin layer influenced by viscosity. However, in rough flow conditions, where there is no distinct viscous layer, the velocity is not influenced by viscosity. Additionally, there is an intermediate transitional phase where both bed roughness and viscosity play a role in shaping the velocity distribution (Liu 2001).

The value of the bottom roughness k_s depends on the presence of ripples (DeVos 2008):

- when no ripples are present $k_s = 2.5d_{50}$, with d_{50} the median sediment grain diameter.
- when ripples are present $k_s = (0.5 - 1)H_r$, with H_r the ripple height

The value of z_0, for the current effect, according to the flow type (DeVos 2008):

$$z_0 = \frac{k_s}{30} + \frac{v}{9u^*} = \begin{cases} \frac{v}{9u^*}, & \frac{u^* k_s}{v} \leq 5 \ \ smooth\ flow \\ \frac{k_s}{30}, & \frac{u^* k_s}{v} \geq 70 \ \ rough\ flow \end{cases} \tag{6}$$

A steady current flowing over a seabed most often has a boundary layer with a thickness that covers a large part of the water depth (DeVos 2008). The velocity equation for a specific depth z (m) is then a function of the friction velocity u_* (m/s), the Von Karman constant k, and the roughness length z_0 (m).

$$U(z) = \frac{u^*}{k} \ln\left(\frac{z}{z_0}\right) \tag{7}$$

Furthermore, the approximation of U_c = $0.4d$ can be used in experimental works, since as the combination of equations (6) and (7), leads to the conclusion that the average flow velocity, U_c, can be measured at approximately 40% of the water depth (0.368d$\simeq$ $0.4d$), counting from the sand bed (Whitehouse 1998).

2.2.2 AMPLIFIED BED SHEAR STRESS AND AMPLIFICATION FACTOR

Installing an offshore wind turbine will change the water flow, causing an increase in bed-shear stress. In order to express the structure's presence, the amplification factor, α, is often used, which is defined as the ratio between the amplified bed shear stress (τ) and the undisturbed bed shear stress ($\tau_\propto$), as shown in Eq. (8)

$$\alpha = \frac{\tau}{\tau_\propto} \tag{8}$$

Although several studies have been performed on the amplification factor, it is hard to find consensual information on the values to be adopted for separated or combined waves and currents . Since the concept is assessed with experimental work and the ratio between the bed shear stresses may be influenced by several factors besides the structure itself, different values are reported (Ferradosa 2011). According to Whitehouse (1998) a typical value of α, for a steady current, is considered to be 4.

As the flow speed increases, the bed shear stress also rises, resulting in higher values of α. These values are usually higher close to the structure where the flow is more disrupted by the new conditions. The amplification factor then starts to decrease as the distance from the structure walls increases. The distribution of the amplification factor is directly related to the pattern of the scour process. This process is more intense in areas with higher values of the amplification factor. In the marine environment, the position of α changes over time due to the varying of currents (Whitehouse 1998).

2.3 THRESHOLD OF MOTION

The threshold of a particle's motion is attained when the driving forces become larger than the stabilizing forces (DeVos 2008). The driving forces are the horizontal drag force F_D, which consists of a friction drag and a form drag, and a vertical lift force F_L (Figure 7). The size of the drag force depends on the particle Reynolds number and the particle's shape.

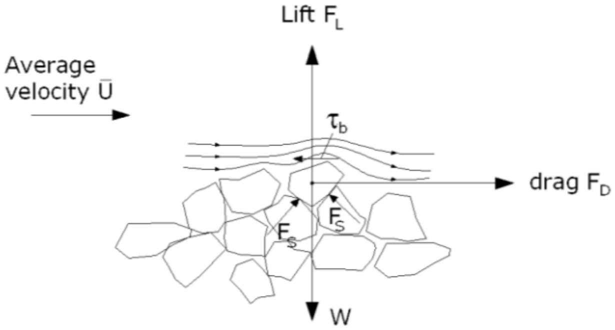

Figure 7. Forces acting on a sediment grain (DeVos 2008).

The bottom bed shear stress can be expressed as a function of the horizontal drag force and of the projected area of the grain on the horizontal plane (A*) (Chambel 2019).

$$\tau_b = \frac{F_D}{A^*} \tag{9}$$

The critical bed shear stress (τ_{cr}[N/m^2]) signifies the threshold at which sediment motion initiates. It characterizes the minimum shear stress required to set sediments in motion. In Soulsby (1997) the non-dimensional parameter for the threshold motion, θ_{cr}, represents the τ_{cr}.

$$\theta_{cr} = \frac{\tau_{cr}}{g(\rho_s - \rho_w)d_s} \tag{10}$$

Shields also proposed the notion of shields curve (Figure 8), which establishes the relation between the critical Shields parameter and the Reynolds number of the particle (Re^*), given in Equation 10.

$$Re^* = u^* \frac{d_s}{v} \tag{11}$$

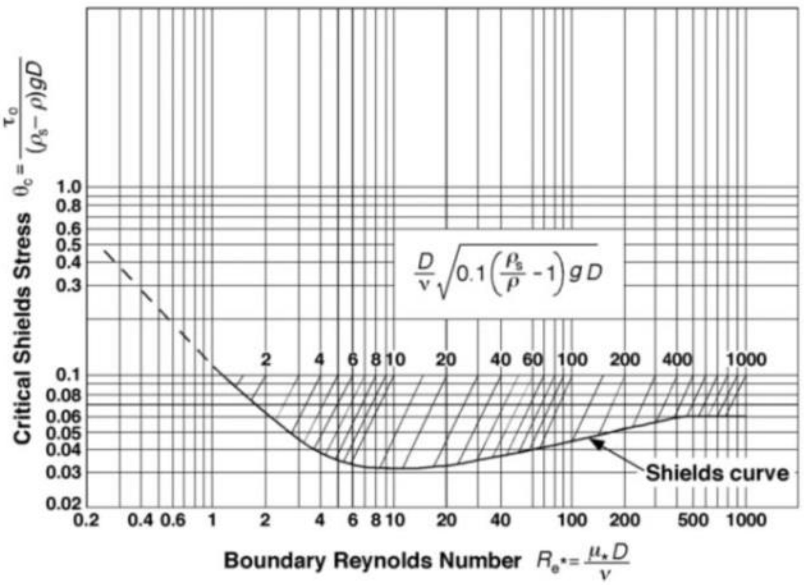

Figure 8. Shields Diagram (Shields 1936)

Since the Shield curve represents a graphical relationship where both variables are interdependent, Shields (1936) proposed the concept of dimensionless grain size (D^*)which modifies the Shields curve (Figure 9).

$$D^* = \left(\frac{g(s-1)}{v^2}\right)^{\frac{1}{3}} d_s \quad (12)$$

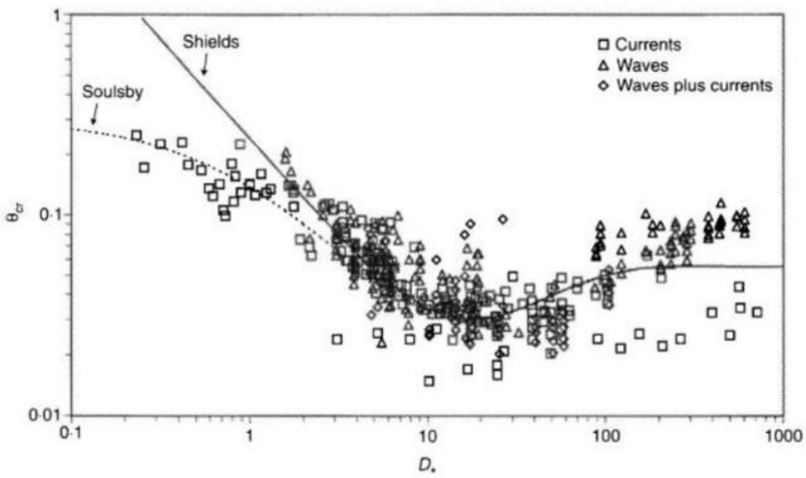

Figure 9. Shields diagram adapted by Soulsby (Miranda 2022)

2.4 CLEAR-WATER SCOUR AND LIVE-BED SCOUR

The scour process, in terms of flow regime, can be classified into two different categories:

- **Clear-Water Regime**: occurs when bed material upstream of a potential scour hole is not in motion, generally because the bed-shear stress upstream of the location is smaller than the critical shear stress of the bed material ($\theta < \theta_{cr}$)

- **Live-Bed Regime:** occurs where the upstream bed-shear stress exceeds the threshold value and the bed material upstream of the scour hole moves ($\theta \geq \theta_{cr}$) (Hoffmans and Verheij 2021)

In Figure 10 it can be seen that in Clear-Water Regime the depth of the scour hole approaches the limit asymptotically, while in Live-Bed Regime the scour increases rapidly with time and then fluctuates about a mean value in response to the bed features that pass by.

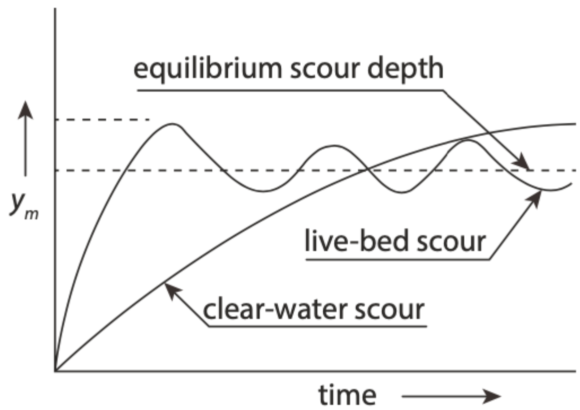

Figure 10. Scour development in clear-water and live-bed scour conditions (Hoffmans and Verheij 2021)

2.5 INFLUENCE OF THE SEDIMENT'S CHARACTERISTICS

The seabed soil characteristics stand as one of the most influential parameters in the scour process around offshore wind structures. In the present research, only non-cohesive soils are considered which vary between 0.062 mm and 2 mm (Rijn 1993).

For the sediments characterization it is usual to define the sediments size using their mean diameter d_{50}, related to the sieve size through which 50 % of the material passes. The grading of the sand grains is characterized by the standard deviation σ defined by the ratio of diameter for which 85% of the material is finer by weight (D_{85}) to diameter for which 15% of the material is also finer by weight (D_{15}):

$$\sigma = \frac{D_{85}}{D_{15}} \tag{14}$$

The grain size distribution is presented in a log-linear distribution plot as we can see in Figure 11.

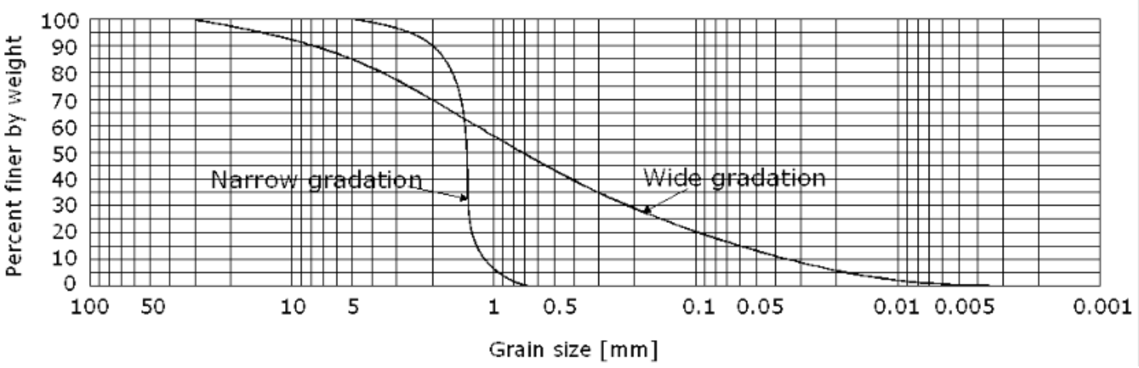

Figure 11. Log probability plot of a wide and narrow grain size distribution(adapted from DeVos (2008))

To differentiate the sediments grading, the ratio D_{85}/D_{15} is used:

- Narrow grading: $D_{85}/D_{15} \leq 1.5$
- Wide grading: $1.5 \leq D_{85}/D_{15} \leq 2.5$
- Very wide grading: $2.5 \leq D_{85}/D_{15} \leq 5$

The mass density ρ_s plays an important role in the stability of sediments. It is defined as the mass m per unit of volume V_s of a sediment:

$$\rho_s = \frac{m}{V_s} \tag{15}$$

The settling velocity W_s of the sediment indicates its transport mode and it can be expressed by the balance between the fluid drag force and the gravitational force (DeVos 2008).

$$W_s = 1.1. [(s-1). g. d_s]^{\frac{1}{2}} \tag{15}$$

Where d_s is considered to be D_{50}, s is the ratio between sediment mass density and the water mass density and $g = 9.81\ m^2/s$.

The presence of larger particles plays a crucial role in the formation of an armoring layer around the monopile foundation. As the bed shear stress increases, the smaller particles are eroded and transported downstream, leaving the coarser materials, which are typically heavier. These larger particles accumulate near the foundation creating a stable layer preventing further erosion. Figure 12 shows an example of an armoring layer formation in a monopile foundation model.

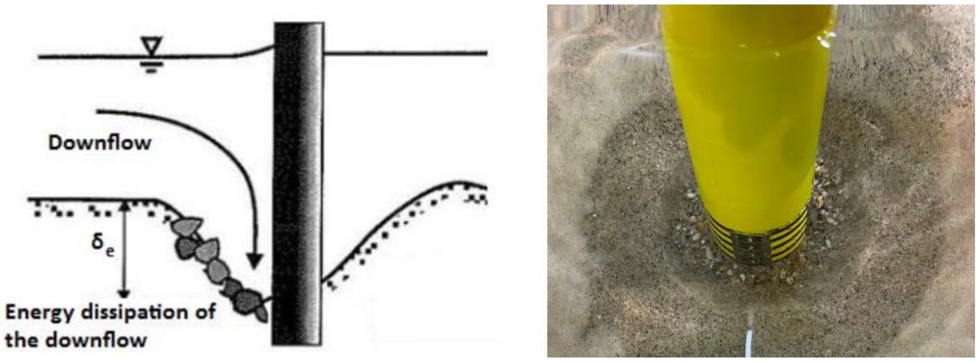

Figure 12. General representation of the armouring layer provided by bigger sediments (left) (Melville and Coleman 2000); Armour effect seen in the laboratorial tests (right)

2.6 SCOUR DEPTH

The scour depth, $S(m)$ is a critical parameter for offshore foundations. It tends to develop asymptotically until its equilibrium, the maximum vertical distance from the surrounding undisturbed bed (Miranda 2022) which can be seen in Figure 13.

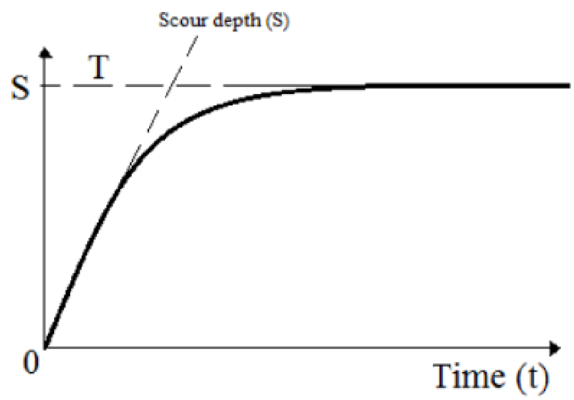

Figure 13. Scour development as function of time (Melville and Chiew 1999)

Because of its significance in foundation design, numerous efforts have been undertaken to consider the evolution of the scour hole over time. Two of the most common prediction approaches are outlined in Eq. (14) and Eq.(15), from Sumer, Christiansen and Fredsoe (1992) and (Melville and Chiew 1999), respectively.

$$S(t) = S_e \left(1 - \exp\left(-\frac{t}{T}\right)\right) \quad 14$$

$$\frac{S(t)}{S_e} = \exp\left[-0.03\left[\frac{U_{cr}}{U}\ln\left(\frac{t}{t_e}\right)\right]^{1.6}\right] \quad 15$$

Where t (s) is the time variable, T(s) is the time necessary to reach a scour depth around 63% of the S_e value, t_e (s) is the time necessary to reach the S_e value, U_{cr} (m/s) is the critical velocity and U (m/s) is the average velocity.

The value t_e can be estimated by Eq.(16) which depends on the water depth (d) and the pile diameter (D_p).

$$t_e(days) = \begin{cases} 48.26\dfrac{D_p}{U}\left(\dfrac{U}{U_{cr}} - 0.4\right) & \dfrac{d}{D_p} > 6 \\ 48.26\dfrac{D_p}{U}\left(\dfrac{U}{U_{cr}} - 0.4\right)\left(\dfrac{d}{D_p}\right)^{0.25} & \dfrac{d}{D_p} \leq 6 \end{cases} \quad (16)$$

The scour depth varies with time but also with the type of flow regime. According to Breusers and Raudkivi (1991), the scour depth and the time scale of the scour process are higher for clear water regime instead of the live-bed regime. This means that the clear-water regime induces a higher equilibrium scour depth value, in the end, but, for the same period of time, before equilibrium stages are reached, scour depth develop at a higher pace for the live-bed regime (Chambel 2019).

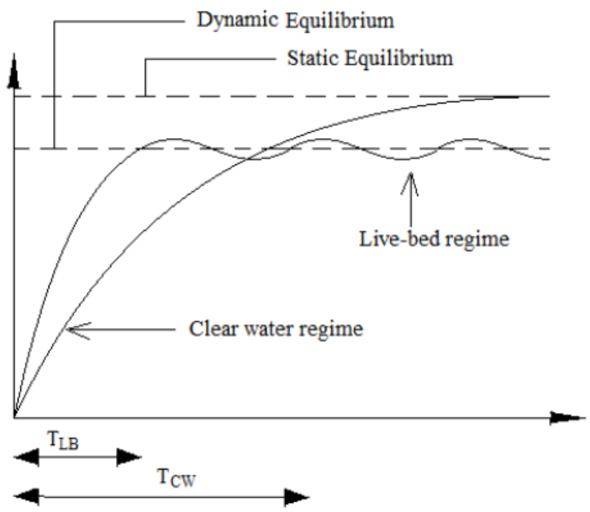

Figure 14. Scour depth evolution and time-scale comparison between live-bed and clear-water scour (Ferradosa 2018)

2.6.1 SCOUR DEPTH FOR CURRENTS

Eq.(17) and Eq.(18) were proposed as prediction equations of equilibrium scour depth under current's attack for a clear-water regime and live-bed regime respectively (Breusers and Raudkivi 1991)

$$\frac{S_e}{D_p} = 2.3K_sK_\sigma K_\alpha K_{si}K_d \quad (17)$$

$$\frac{S_e}{D_p} = 2.3K_sK_\alpha K_{si}K_d \quad (18)$$

where K_s corresponds to the shape factor, K_σ to a factor dependent of the grain size distribution σg=d_{84}/d_{50}, K_α to the pile alignment factor, K_{si} to the pile size factor and K_d to the flow depth factor. For cylindrical monopiles, K_s and K_α are equal to 1. For values of d/D_p>3 K_d is equal to 1 and for high values of D_p/d_{50}, K_{si} is equal to 1. For values of d/D_p≤3, De Vos (2008) refers to the the determination of the K_d value (Chambel 2019).

Other equations, presented by authors like Sumer et al.(1992), are used for live-bed regime (Eq.(19)). Whitehouse(1998) presented Eq.(20) for clear-water regime depending on the Shields and critical Shields parameter.

$$\frac{S_e}{D_p} = 1.3 + \sigma_s \qquad 19$$

$$\frac{S_e}{D_p} = 1.3\left[2\sqrt{\frac{\theta}{\theta_{cr}}} - 1\right] \qquad 20$$

With σ_s equal to 0.7.

2.7 SCOUR EXTENT

For non-cohesive soils, the scour hole tends to be shaped like an asymmetrical cone as the one presented in its vertical profile (Figure 15) which is characterized by upstream and downstream slopes, α_{up} and α_{down}, respectively, and its total scour extent W (DeVos 2008).

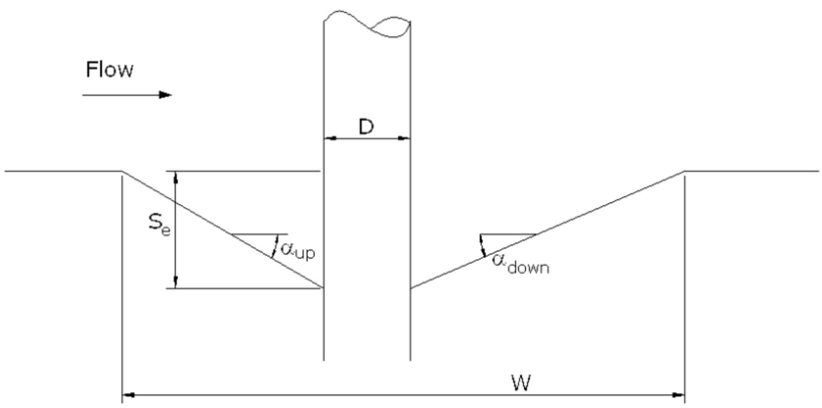

Figure 15. Scheme of scour dimensions (DeVos 2008)

$$W = D_p + S_e\left[\cot(\phi_{up}) + \cot(\phi_{down})\right] \qquad 21$$

Where α_{up} is the internal friction angle of the sediments ϕ_i and α_{down} the downstream angle that tends to be approximately half of the upstream.

2.8 SCOUR TESTS REVIEW

To better analyze and interpret the results of the present research it is important to compare them with previous works and tests performed by other authors.

For currents, contributions provided by Melville and Raudkivi (1977), Melville and Sutherland (1988) have shown that the ratio of scour depth to diameter (S/D) is influenced by several factors. Specifically:

- Increases with h/D;
- Increases with Shields parameter θ;
- Decreases with increasing sediment gradation
- Increases with increasing, D/d;
- Increases with the Froude number.

Depending on these parameters, the scour depth (S) tends to fall in the range of 1-2.5D.

Research on layered seabed configurations was performed in Porter, Harris et al. (2013), Ferradosa (2018) and WenGang and FuPing (2014). In these studies, different sand grain sizes were considered and tests were made for different sand types. Table 1 summarizes the test conditions and scour results from the previous scour tests.

Table 1. Review on existing scour tests in layered beds

Author	Porter, Harris et al. (2013)				Ferradosa (2011)		Wang, Yuan et al. (2022)	
$D_{50}(mm)$ range	0.2-0.6	0.2-0.6	0.2-0.6	0.2-0.6	0.17-0.64	0.17-0.64	0.15-2	0.15-0.5
$D(m)$	0.04	0.04	0.04	0.04	0.04	0.04	0.03	0.03
U_c(m/s)	0.19	0.19	0.19	0.19	0.22	0.22	0.20	0.20
Sand type	Fine and Coarse	Fine and Coarse	Fine	Coarse	Fine and Coarse	Fine and Coarse	Fine and Coarse	Fine and Coarse
Upper layer (m)	Fine Sand 0.10	Fine Sand 0.40	-	-	Fine Sand 0.04	Coarse Sand 0.04	Fine Sand 0.01	Coarse Sand 0.01
Lower layer (m)	Coarse Sand	Coarse Sand	-	-	Coarse Sand 0.06	Fine Sand 0.06	Coarse Sand	Fine Sand
Water Depth (m)	0.17	0.17	0.17	0.17	0.17	0.17	0.15	0.15
S/D	1.08	1.18	1.5	0.93	1.6	1.7	0.5	0.7

It is worth highlighting the results obtained by Ferradosa (2011). In the author's experiments a higher scour depth was obtained when coarse sand was overlaying fine sand. The results can be found in Figure 16 and are going to be discussed in Chapter 4.

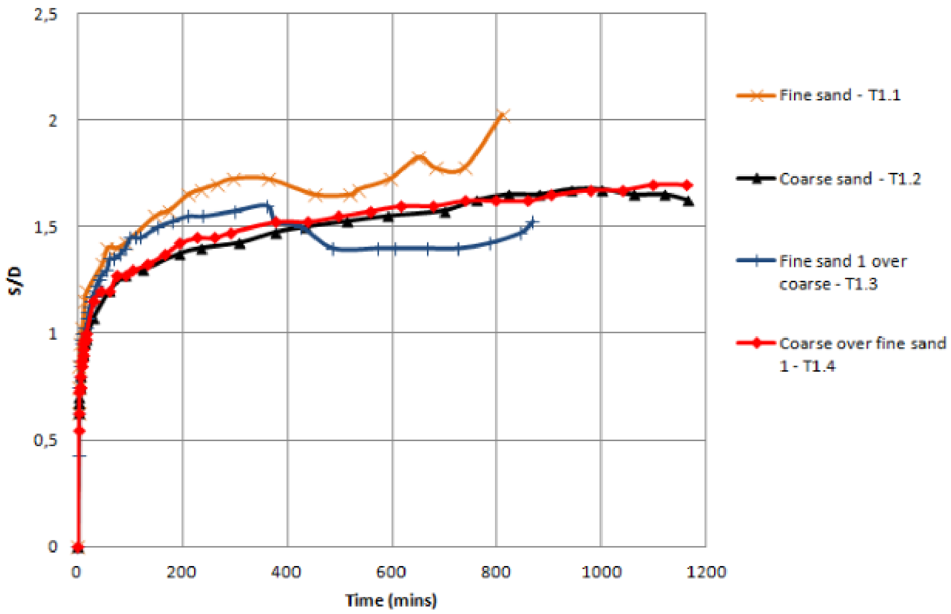

Figure 16. Scour depth over time curve (Ferradosa 2011)

According to the results obtained by Wang, Yuan et al. (2022), the scour development curve in double-layered soil can be mainly categorized into four typical regimes presented in Figure 17.

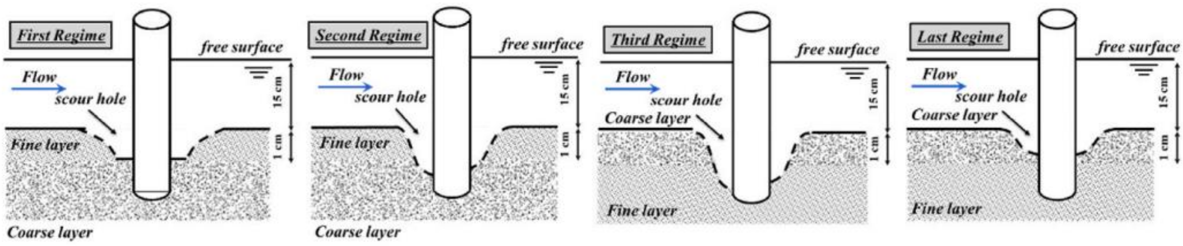

Figure 17. Influence of the particle size of the overlying sediment on the final scour depth (Wang, Yuan et al. 2022)

In the first regime, $r_d < d_{over}/d_{cr,over} < 1$ the flow is able to erode the entire layer of the overlaying sediment but cannot erode the particles in the. Underlying layer.

In the second regime $d_{over}/d_{cr,over} < r_d < 1$ the flow velocity reaches or exceeds the initiation velocity of the particles in the underlying sediment layer and erosion continues to develop until an equilibrium state is reached.

In the third regime $1 < r_d < d_{over}/d_{cr,over}$ the coarse particles are winnowed by the coming flow, and some of the overlying coarse particles will be deposited in the scour hole and mixed with the underlying fine particles, forming a mixed armor layer. With scour development, the exposed water-soil interface will become a water-armored layer interface, which will prevent additional erosion. When the equilibrium status is reached, the final scour depth will be less than in the single fine soil layer.

In the fourth regime, $1 < d_{over\prime}/d_{cr,over} < r_d$, where the particle size of the overlying sediment is larger than $d_{over\prime}$, the overlying layer is not totally eroded, and the scour process is similar to a single sediment layer, resulting in the same scour depth as a singles layered sediment and the scour depth decreases as the particle size increases (Wang, Yuan et al. 2022).

2.9 PHYSICAL MODELING: SCALE AND MODEL EFFECTS

To support their investigations, researchers use numerical, laboratory/physical and composite modelling. In the present dissertation, physical modeling will be used. The main advantage of this approach is the ability to control, adjust and separate different types of conditions. A small-scale laboratory physical modelling studies remains a reliable tool for designing and testing of various types of structures affected by scour phenomena (Hughes 1993).

Although these advantages, and since these studies use reduced scale model of the actual prototype structure, it may lead to disparities between prototype and laboratory model. These disparities are caused by model and scale effects. According to DeVos (2008) and Frostick, McLelland and Mercer (2011)

- **Model Effects**: emerge from an incorrect reproduction of the prototype situation in the model set-up of the laboratory, promoting non-existing or unrealistic prototype boundaries and conditions;

- **Scale Effects:** occur due to force ratios which are not identical between the model and the prototype, leading to oversimplifications.

Table 2. Model and Scale effects for physical scour model

Effects	Example
Model Effects	Blockage and side walls effects, sediment supply, bed roughness
Scale Effects	Influence of the Reynolds number, sediment scaling,

Model effects like the side wall effects and the blockage effects of the flume, the sediment supply and the bed roughness should be considered. When considering scour studies in the flume, it is important to think about the effects of the proximity of the side walls. When the flow is accelerated due to a reduction in the cross -sectional area, blockage effects occur (Porter 2016). According to Whitehouse (1998) the blockage effects can be disregarded if:

$$\frac{A_{(model)}}{A_{(flume)}} \leq 0.167 \tag{22}$$

Where $A_{(model)}$ is the cross-sectional area of the structure and $A_{(flume)}$ is the cross-sectional area of the flume. The proximity of the structure to the flume's side wall can also have an impact on the test, having an influence on the flow acceleration and changing the wake structure. Sumer and Fredsøe (1997) presented that the wall effect can be negligible if the distance to the wall is more than 1-2 pile diameters in currents.

Differences in the bed roughness can also have effects in the tests. If the roughness is not constant along the flume the boundary layer velocity would be affected, leading to changes in the values of the bed shear-stress and in the friction velocity contributing to an inexactness (Ferradosa 2011).

Furthermore, since the flume operates in a closed circuit and the water is always recirculating, sand that may pass through the sediment retention chamber can enter the hydraulic circuit and become suspended in the water entering upstream. This could affect the sediment balance in the study area.

More attention is given to scale effects as they are believed to have more influence on the results than the model effects. The most important scale effects are related to the inability of sediment scaling. When scaling sediments, as the diameter decreases, they obtain cohesive properties. This poses a problem, since the non-cohesive properties of the soil should be kept, which is the most common in offshore monopiles.

Sediments cannot be scaled with geometric length scale but can be scaled using the dimensionless Shields parameter presented in Eq.(3). Both the diameter and density of the model bed material are variables that can be selected and as a result both sand and lightweight granular materials can be considered when selecting the model scale (Whitehouse 1998).

To ensure similitude in the model is necessary that geometric, kinematic and dynamic similarity must be maintained. The correct scaling of currents in laboratory studies must preserve the Froude number (Fr)- number that conserves gravity effects- and the Reynolds number (Re)-number that conserves viscous effects, respectively defined in Eq.(23) and Eq.(24):

$$Fr = \frac{U}{\sqrt{gh}} \tag{23}$$

$$Re = \frac{UD_p}{v} \tag{24}$$

However, is not possible to scale both numbers at the same time because of the preservation of the geometric scale. The majority of the hydraulics models are scaled according to the Froude number, where Froude number in the prototype is equal to the model's Froude number (Hughes 1993).

2.10PREDICTING METHODS FOR THE EQUILIBRIUM SCOUR DEPTH

2.10.1 MELVILLE & COLEMAN (2000) APPROACH

This method can be applied both to situations in clear-water regime and live-bed regime. Takes into account a considerable amount of variables that are involved in the scour process.

According to Melville and Coleman (2000), Eq.(27) provides an estimation value for the equilibrium scour depth:

$$S_e = K_h K_I K_D K_s K_\alpha K_t \tag{27}$$

In cylindrical piles the factor K_h, which represents the effect of the pile dimensions and the water depth, can be obtained as:

$$K_h = \begin{cases} 2{,}4D_p & ,if \quad \dfrac{D_p}{d} \leq 0.7 \\ 2 \times \sqrt{dD_p} & ,if \quad 0.7 < \dfrac{D_p}{d} \leq 5.0 \\ 4{,}5d\ , & ,if \quad \dfrac{D_p}{d} > 5.0 \end{cases} \tag{28}$$

K_I is the factor used to represent the flow intensity and is obtained by the following equation. For uniform sediments $U_a = U_c$

$$K_I = \begin{cases} \dfrac{U-(U_a-U_c)}{U} & ,\dfrac{U-(U_a-U_c)}{U} < 1 \\ 1 & ,\dfrac{U-(U_a-U_c)}{U} \geq 1 \end{cases} \tag{29}$$

Factor K_D, takes into consideration the effect of the sand particles dimension:

$$K_D = \begin{cases} 0.57\log\left(2.24\dfrac{D_p}{d_{50}}\right) & ,\dfrac{D_p}{d_{50}} \leq 25 \\ 1 & ,\dfrac{D_p}{d_{50}} > 25 \end{cases} \tag{30}$$

The factor K_s value for a circular pile is 1.

The influence of the attack angle of the flow towards to the pile is evaluated by K_α factor, which for cylindrical piles is equal to 1.

Factor K_t describes the time's influence in the scour hole extent and the scour depth. For live-bed regime situations the equilibrium scour depth is quickly achieved and usually the value is considered to be equal to 1. However for cylindrical piles in clear-water regime the value assumed for this parameter is given by Eq.(31) and an estimative for t_e is obtained by Eq.(32):

$$K_t = e^{-0.03\times\left|\frac{U_c}{U}\times\ln\left(\frac{t}{t_e}\right)\right|^{1.6}} \tag{31}$$

$$t_e = \begin{cases} 48.26\dfrac{D_p}{U}\left(\dfrac{U}{U_c}-0.4\right), \dfrac{d}{D_p} > 6\ and\ \dfrac{U}{U_c} > 0.4 \\ 30.89\dfrac{D_p}{U}\left(\dfrac{U}{U_c}-0.4\right), \dfrac{d}{D_p} \leq 6\ and\ \dfrac{U}{U_c} > 0.4 \end{cases} \tag{32}$$

2.10.2 BREUSERS ET ALL (1977)

In Breusers, Nicollet and Shen (1977):

$$S_e = f\left(\frac{U}{U_c}\right)\left[2\tanh\left(\frac{d}{D_p}\right)\right]K_s K_\theta D_p \tag{33}$$

The function presented is obtained by Eq.(34):

$$f\left(\frac{U}{U_c}\right) = \begin{cases} 0 & if\ \frac{U}{U_c} \leq 0.5 \\ \left(2\frac{U}{U_c} - 1\right) & if\ 0.5 < \frac{U}{U_c} < 1 \\ 1 & if\ \frac{U}{U_c} > 1 \end{cases} \tag{34}$$

2.10.3 FROELICH DESIGN (1988)

According to Froelich (1988):

$$S_e = 0.32 D_p \emptyset Fr^{0.2}\left(\frac{W}{D_p}\right)^{0.62}\left(\frac{d}{D_p}\right)^{0.46}\left(\frac{D_p}{d_{50}}\right)^{0.08} \tag{35}$$

W represents the pile width perpendicular to the direction of the flow. The values of $\emptyset$ correspond to the pile shape factor and the suggested values can be observed in Figure 18.

Pile shape sketch	Pile shape	Ø
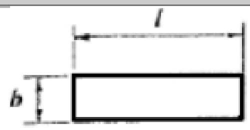	Rectangular Shape	1.3
	Rounded end	1.0
	Angular ends	0.7

Figure 18. Pile shape factor, Ø (Froelich 1988)

There is a variety of formulas and it is expectable that the estimations for the scour depth will not match each other. Each approach considered different variables. Prediction methods of Melville and Coleman (2000), Froelich (1988) and Breusers, Nicollet and Shen (1977) take into account the fact that the scour process depends on variables like the threshold velocity, the sediment dimensions and water depth.

For more complex situations like layered beds, further research is needed.

3 EXPERIMENTAL STUDY

This research project involved experimental work to evaluate the scour process around a cylindrical uniform pile under steady current flow conditions in a current flume. The study focused on providing detailed data on the depth, shape, and extent of the resulting scour holes. The experiments were conducted with the monopile founded in two types of sand isolated and then for layered sediment beds to develop a comprehensive and thorough understanding of the scour process in simple cases, and to extend and compare this knowledge to more complex situations.

This chapter delves into an analysis of the conducted experiments, providing a comprehensive description of the laboratory facilities and the experimental methodologies employed to execute the scour tests. Additionally, delineates the preliminary experiments undertaken to define the initial conditions for the scour experiments, along with the tests conducted to refine the experimental design. It also elaborates on the preceding calculations and methodologies utilized to assess the preliminary laboratory conditions. Furthermore, a comprehensive presentation and description of the measuring equipment and techniques employed in this research project is provided.

3.1 CURRENT FLUME

The experimental work was conducted at the Faculty of Engineering of University of Porto (FEUP), in the Hydraulics Laboratory of the Civil Engineering Department (Hydraulics, Water resources and Environment Division (SHRHA)). The facility provides a small flume for experimental work, capable of replicating marine and fluvial conditions with the layout represented in Figure 19.

The small size of this flume offers advantages. It allows for quicker setup of each experiment and provides ideal conditions for conducting tests on a more practical and controlled scale. However, it is important to note that the results from these experiments and their respective analysis must account for the effects induced by scaling issues.

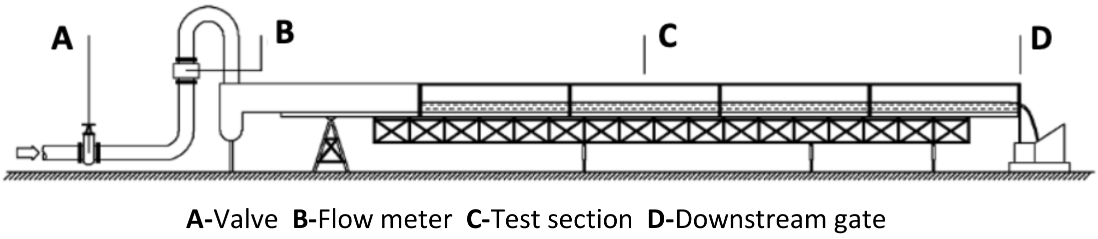

Figure 19. Scheme of FEUP's small flume (Secção de Hidráulica)

The flume is 17 m long, 40 cm wide, and 60 cm deep. Water is pumped into the upper reservoir which supplies the canal gravitationally from two reservoirs located at a lower level (beneath the floor of the laboratory area). These reservoirs are 6 m wide, 8 m long, and 2.5 m high. Two pumps, arranged in parallel, pump water from these reservoirs to a constant level head reservoir with dimensions of 12.3 m by 3.3 m and a depth of 1.3 m, situated 3.02 m above the flume. The flume is supplied by a pipeline equipped with a regulation valve and a flowmeter that displays the discharge flow, allowing for flow regulation. To control the water depth, the flume is equipped with an electrical gate at the downstream end.

Figure 20. Flume general views

To create the necessary conditions for performing offshore experimental tests, adaptations and upgrades were made to the flume. An approach ramp was designed and constructed to ensure a smoother transition of the flow before it reaches the test section (Figure 21).This ramp ensures that the water flow is steady and uniform, reducing turbulence that could affect the accuracy of the experiment. The approach ramp (Figure 22)**,** made of wood, has a 1/10 slope and a 3 m length before and after the sediment box.

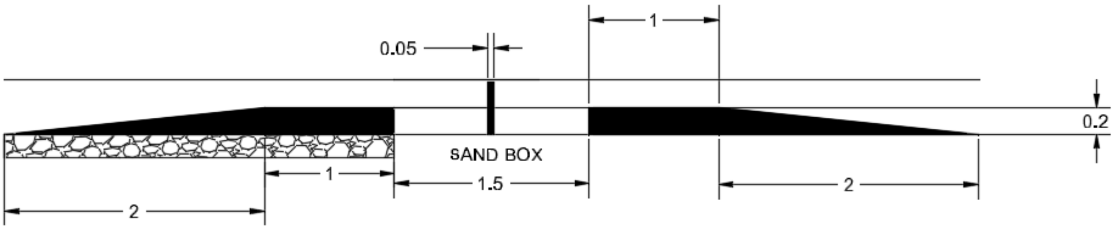

Figure 21. Approach ramp's Scheme in SI units (meters)

Figure 22. Different views of the approach ramp

Furthermore, in order to guarantee a smooth transition of roughness conditions between the false bed and the sediment box, the surface of the false beds section was covered with sand particles. These particles were glued to the false bed top surfaces to avoid the particle movement during the tests (Figure 23).

Figure 23. False sand bed

The sediment box represented a section of the flume's length where the monopile foundation would be centrally placed and embedded within sediments. This setup allowed for the observation and evaluation of the scour process. The box measured 1.5 m in length, 20 cm in depth and 40 cm in width.

Figure 24. Sediment box

In a scour test, a significant amount of sand is often carried downstream, potentially entering the internal hydraulic circuit and causing major issues. This can lead to excessive wear on the pump group and clogging in the pipe sections due to sediment accumulation. To prevent sand from entering the hydraulic circuit and damaging the pumps, a sediment retention chamber was installed at the end of the flume (Figure 25).

Figure 25. Sediment retention chamber

3.2 MONOPILE PHYSICAL MODEL

For the experimental study of the current dissertation a monopile foundation physical model was used to replicate common marine infrastructures of support for offshore renewable energy. A cylindrical pile with a diameter of $D_p = 0.05$ m was used (Figure 26). This acrylic pile model consists of 2 detachable parts and a square plate at the base to add stability to the model and to facilitate its use. The first part that is attached to the base is 19 cm high and the other part is 61.3 cm.

Figure 26. Parts of the pile used

It is important to mention that the pile size adhered to the practical guidelines established by Whitehouse (1998):

- **Rule for Blockage-** the ratio of the area of the flume to the area of the model needs to be at least 6, to avoid a significant blockage effect leading to the constriction of the flow and to a direct effect on the scour depth values
- **Water depth vs Pile diameter rule-** The effect of water depth on the scour depth at cylindrical piles is agreed to be negligible for values of the ratio $h/d > 3$. For these set of tests the pile diameter was 5 cm while the water depth was 15 cm, having a $h/d = 3$ being in the limit

In order to maintain the pile in a stable vertical position and prevent any sliding or rotational movement, the monopile was attached to a squared PVC base with a thickness of 1.4 cm. Subsequently, the pile, along with the base structure, was centered within the sediment box. Then, the sediment was added to the sediment box, providing additional stability to the monopile.

Smoothing the sand bed is important to allow the levelling of the sand layers used in each experiment. For this purpose, a sand smoother was used. This device had a wood handle and attached to this structure there was a plastic ruler which would provide the horizontal smoothed shape of the bed (Figure 27).

Figure 27. Sand smoother

Using this device is essential because it helps eliminate ripples on the sand bed. These ripples can cause inaccuracies in measuring scour depth. If not smoothed out, material from the ripples upstream can fall into the scour hole, leading to fluctuating and unreliable S_e values (Ferradosa 2011).

3.3 SOIL CHARACTERISTICS

The aim of this study was to analyze the scour phenomenon of soils with different characteristics. In the present research three sands were tested, one test of uniform sand and four in layered tests.

Table 3. Uniform sediment's characteristics

Sediment	**Grading**	d_{15}	d_{50}	d_{85}	$\rho_s(kg/m^3)$	σ_D
Fine Sand 1	Narrow	0.200	0.273	0.360	2650	1.8
Fine Sand 2	Wide	0.106	0.250	0.500	2650	4.7
Coarse Sand	Normal	0.319	0.484	0.649	2650	2.03

Figure 28. Sand used in the experiment

The Fine Sand 1 material was SP 55 silica sand. According to Silva(2010) this sand has a mean diameter of d_{50}=0.273mm and a density of $\rho_s = 2650\ kg/m^3$. A sieving sediment analysis was performed according with the Portuguese Norm NP EN 933-1. This sand was sieved with a 1mm sieve in order to remove some bigger particles. The sediment analysis is giving in Table 4.

Table 4. Sediment analysis for the Fine Sand 1

Sieve Opening (mm)	Retained (%)	Cumulative Retained (%)	Cumulative passing (%)
1.000	0.0	0.0	100.0
0.710	0.0	0.0	100.0
0.500	0.0	0.0	100.0
0.355	4.67	4.67	95.33
0.250	58.20	62.87	37.13
0.180	29.66	92.53	7.47
0.125	7.12	99.65	0.35
0.090	0.34	99.99	0.01
0.063	0.01	100.0	0
<0.063	0.0	100.0	0

The Fine Sand 2 was provided by the SHRHA. The Coarse Sand was obtained from Fine Sand 2 using a 2.36 mm sieve to remove the larger particles and a 0.115 mm sieve to increase the d_{50} of the sand (Figure 29).

Figure 29. Sieves of 0.115, 1 and 2.36 mm used

As in the first sand, an analysis was performed according to the Portuguese Norm NP EN 933-1. The sediment analyses were performed in the Construction Materials Testing Laboratory (LEMC) from FEUP.

Samples of each sand were first dried and then subjected to a quartering process to reduce the size of the samples and obtain the required quantity. According NP EN 933-1, a minimum of 200 g of sand was required.

Figure 30. Instrument used for quartering

After quartering, the subsamples were sieved for 15 minutes on a mechanical sieve shaker using a standard set of sieves arranged in descending order of mesh size (Figure 31). The order of the sieves was 8.0, 4.0, 2.0, 1.0, 0.500, 0.250, 0.125 and 0.063 mm.

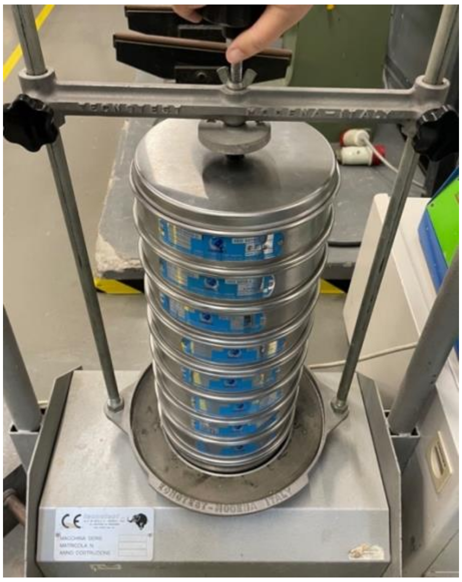

Figure 31. Mechanical sieving process

Each sieve is carefully weighed with the sample retained on it. The percentage by mass for each size fraction is then calculated relative to the starting sample mass and reported as particle size distribution. Table 5 and Table 6 show the results from the sediment analysis for Fine Sand 2 and Coarse Sand respectively.

Table 5. Sediment analysis for the Fine Sand 2 performed in the LEMC

Sieve Opening (mm)	Retained (%)	Cumulative Retained (%)	Cumulative passing (%)
90.0	0.0	0.0	100.0
63.0	0.0	0.0	100.0
31.5	0.0	0.0	100.0
16.0	0.0	0.0	100.0
8.0	0.0	0.0	100.0
4.0	0.0	0.0	100.0
2.0	0.0	0.0	100.0
1	0,2	0.2	99.8
0.500	13.8	14.0	86.0
0.250	35.4	49.4	50.66
0.125	30.7	80.1	19.9
0.063	16.1	96.2	3.8
P	3.3	99.6	0.4

Table 6. Sediment analysis for the Coarse Sand performed in the LEMC

Sieve Opening (mm)	Retained (%)	Cumulative Retained (%)	Cumulative passing (%)
90.0	0.0	0.0	100.0
63.0	0.0	0.0	100.0
31.5	0.0	0.0	100.0
16.0	0.0	0.0	100.0
8.0	0.0	0.0	100.0
4.0	0.1	0.1	99.9
2.0	2.8	2.8	97.2
1	9.4	12.2	87.8
0.500	34.5	46.7	53.3
0.250	53.2	99.8	0.2
0.125	0.0	99.8	0.2
0.063	0.0	99.8	0.2
P	0.0	99.8	0.2

The following Figure 32 presents the grading curves made for each type of sand after the sediments analyses.

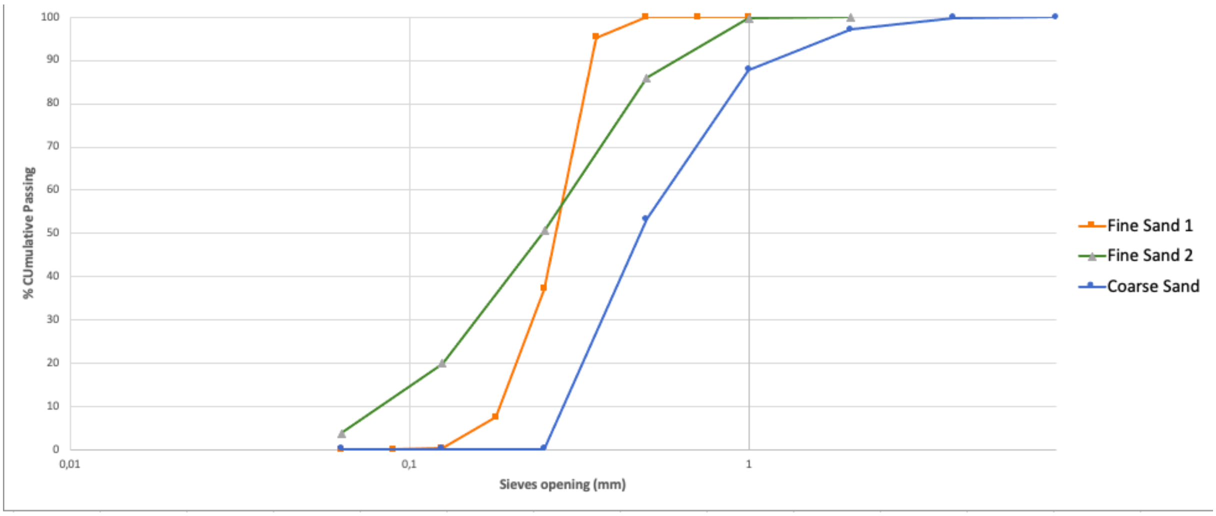

Figure 32. Grading Curves for the sediments used in the scour tests

3.4 MEASUREMENT TECHNIQUES

3.4.1 FLOW VELOCITY MEASUREMENTS

In order to verify the flow velocity an Accoustic Doppler Velocimetry (ADV) was used. The device used was designed by Nortek AS and it was the model Vectrino, with an accuracy of 1 mm/s and with a max sampling rate of 200Hz and with an accuracy of ± 1 mm/s.The equipment is fixed to a metal support structure as it can be seen in Figure 33.

Figure 33. ADV and support structure

First a velocity profile was taken using the ADV, to confirm the flow velocities using only the pipeline connected to the functioning flowmeter. An intake flow of 10.8 L/s was chosen regulating the electrical gate at the end of the flume until a flow depth of 15 cm is reached (Figure 34).

Figure 34. Flowmeter (Left); Electrical gate (Right)

To build the velocity profile, the ADV probe was lowered until it was submerged and 5 cm above the bed. The next measurements were taken for each 1 cm until the water surface. To collect data, the ADV is connected to the data acquisition system *VectrinoPlus*. The results obtained are presented in Figure 35.

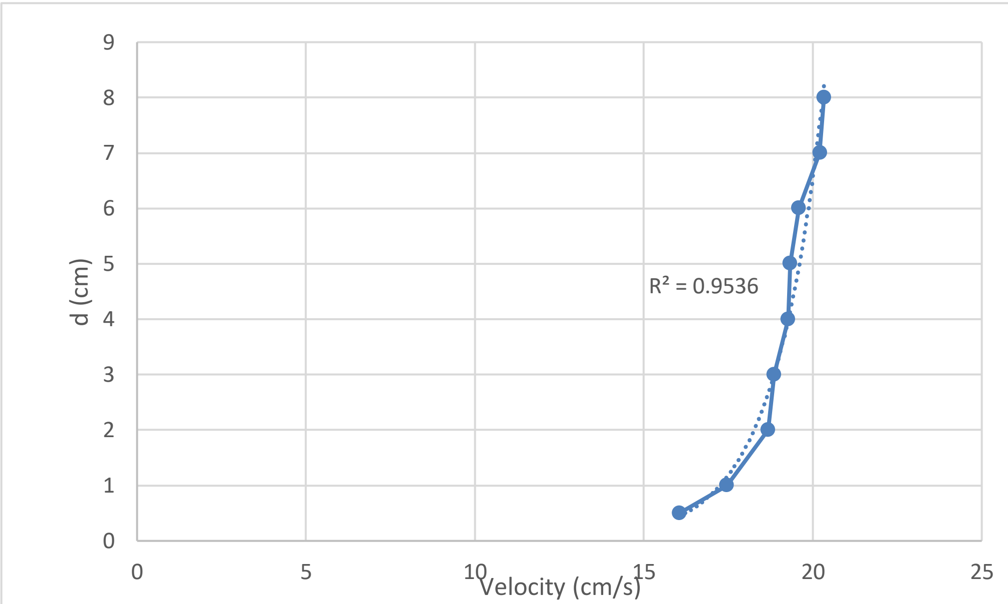

Figure 35. Velocity profile

In all measurements seeding was added to the water in order to have better conditions. By analyzing the trendline of the velocity profile, it can be seen that the exponential trendline fit the profile ($R^2 = 0.953$), having a high correlation value. Measured values were considered valid when the following conditions were verified.

- **Signal-to-Noise Ratio** (SNR) were higher than 15, so the measured velocities are above the noise level;
- **Correlation** was higher than 90%, which indicates that the signal quality is enough for the accuracy of the velocity measurements (NORTEK 2018).

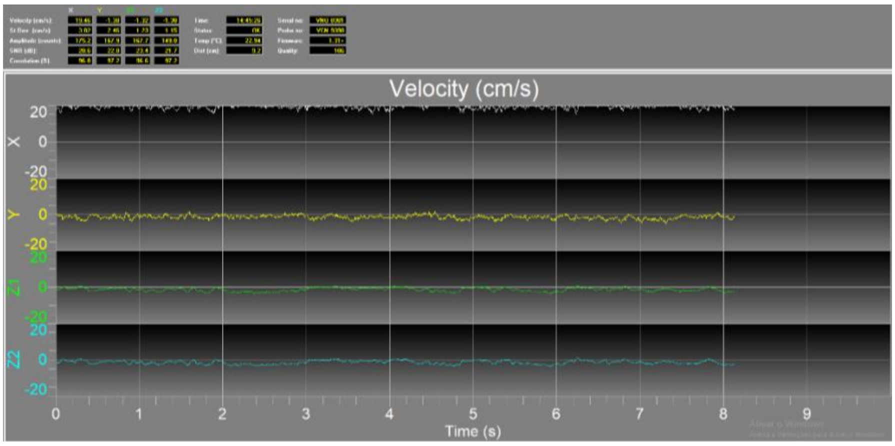

Figure 36. Accurate velocity measurement

3.4.2 SCOUR HOLE CHARACTERIZATION

The scour hole was characterized by utilizing two distinct methods. Firstly, a laser scanner was employed to record the beginning and end of each test. This method allowed for a comprehensive assessment of the scour hole. Additionally, the scour depth was directly measured during the test by reading a ruler placed on the upstream side of the flume. This direct measurement provided valuable data regarding the scour development overt time. By combining these two approaches, a detailed understanding of the scour process and its effects on the seabed and monopile foundation was achieved.

For each test, two sets of 4 laser scans were performed, the first set at the beginning of each test and the second set after the test, in order to compare the scour development. The laser scans were performed using the FARO laser scanner device.

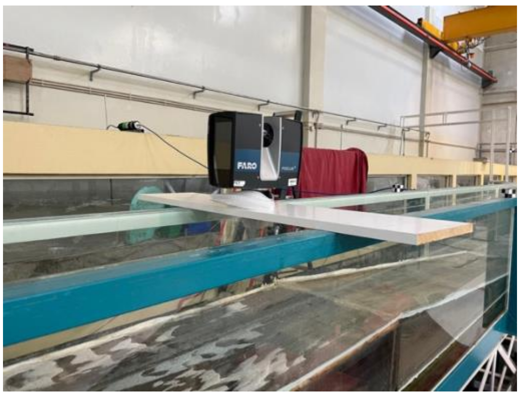

Figure 37. FARO laser scanner

To create a full high-resolution scan, for each set of laser scanning, 4 scans were performed from 4 different placements. Two laser scans were recorded upstream of the sediment box, with one positioned on each side of the flume. The remaining two laser scans were recorded in the symmetrical positions, but downstream of the sediment box as it can be seen in Figure 38.

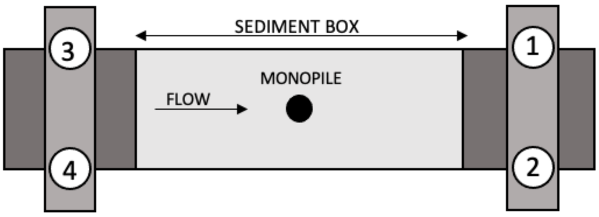

Figure 38. Flume layout top view with the lasers scan placements

3.4.3 POST PROCESSING

The laser scans recorded in each test were merged. This process is performed in RECAPE PRO. To superimpose each laser scans, artificial targets must be strategically placed. In the present setup, six targets were positioned along the flume: one at each side, one at the end of the facilities, and another near the upstream wall. Despite having nine targets in the laboratory, only three were required for each laser in the software. These targets, shaped as squares from a checkerboard pattern (as shown in Figure 39), serve as reference points for accurate alignment and registration of the scans. It's important to note that in each laser scan, the upper part of the pile was consistently detached before capturing the scans.

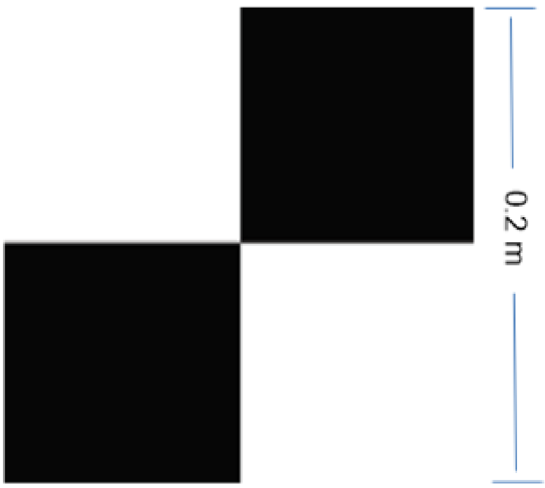

Figure 39. Example of a target

Figure 40. Targets placements

At the end of each test and after the scans were finalized, the eight scans were imported to RECAPE PRO software where it was possible to process, merge, and generate point clouds. In each pair of scans was essential to identify a minimum of 3 targets to merge all the scans (Figure 41).

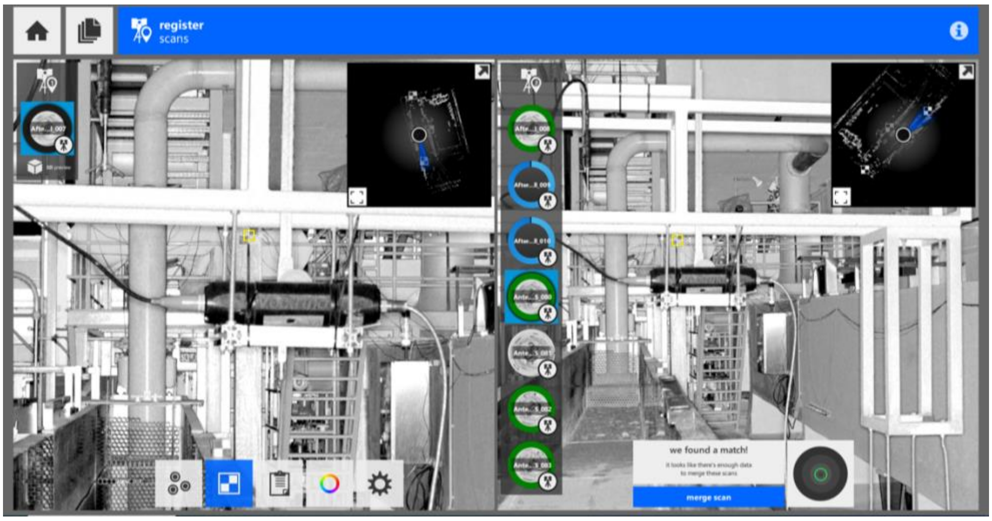

Figure 41. RECAPE software

Once merged, a point cloud of the entire laboratory is created. To make easier the extracting and subsequent processing, only a clipped box of the study area was exported (Figure 42).

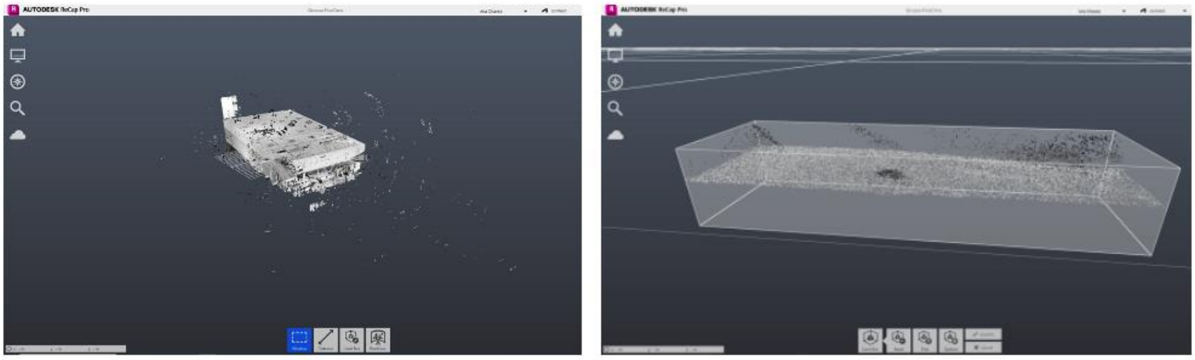

Figure 42. Point Cloud of the laboratory (left); Chosen clip box (right)

In order to analyze the point clouds created in the RECAPE PRO software, the clipping boxes exported were imported into the CloudCompare software. CloudCompare is a 3D point cloud processing software capable of comparing two 3D point clouds. The clipping boxes were exported to E57 files and imported to CloudCompare in order to analyze the obtained scour hole. After the cleaning of unwanted points, a scour map was generated using the option "*cloud-to-cloud distances*" between the final scans and the initial scans. This tool computes the point distances between the initial and final bathymetries in the XYZ axis.

After the cloud-to-cloud distances were computed, the cloud was analyzed and adjusted to facilitate the visualization of scour patterns and zones of deposition. The color scale saturation range was adjusted in order to identify the deposition zones with color red and the scour zones with the color blue.

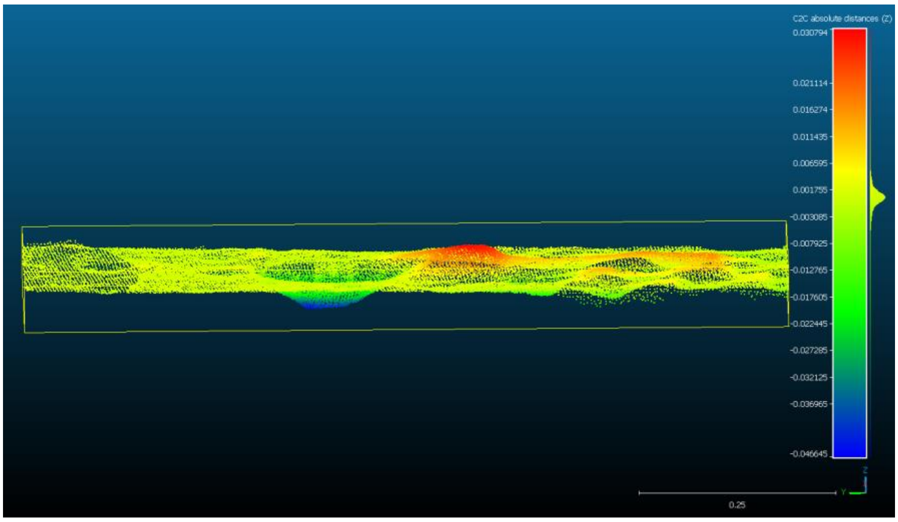

Figure 43. Test scan after the "cloud-to-cloud distances"

After processing the point cloud, some unnecessary points around the pile were removed, creating a hole in the point cloud. This hole was filled in using the "*kriging"* interpolation option, obtaining then the scour map patterns.

3.5 LABORATORY TESTS

3.5.1 EXPERIMENTAL PROCEDURES

The following explanation regarding the experimental procedures was design with the main purpose of creating a standard set of actions so that the scour tests are able to be repeated, in further scour analysis and to diminish the human errors associated:

1. Place the pile in the center of the sediment box;
2. Fill the sediment box with sand to desired level;
3. Smooth the sand-bed;
4. Perform the initial 4 laser scans;
5. Attached the upper part of the pile;
6. Insert the protective cover
7. Slow filling the flume, by opening the regulation valve, until reaching the desired water depth of 15 cm;
8. Take readings from the same place of the pile, every 30 seconds for the first 20 minutes and then less frequently over time;
9. Let the test run for 13 hours or until the scour equilibrium depth is reached;
10. Slow emptying of the flume until the sand box surface is totally dry;
11. Detach the upper part of the pile;
12. Perform the last 4 lasers.

Figure 44. Photo's sequence of the experimental procedure

3.5.2 VELOCITY CHARACTERIZATION

Attempting to define the threshold velocity for the set of conducted experiments, some preliminary tests and analysis were made.

To be able to achieve the maximum scour depth, the worst scenario in terms of the structure to collapse, the velocity used should be as near as possible to the critical values for the threshold of motion. For this study an estimation of the velocity was made using Eq. (25) from Soulsby (1997):

$$U_{cr} = 7\left(\frac{h}{d_{50}}\right)^{\frac{1}{7}} [g(s-1)d_{50}f(D_*)]^{\frac{1}{2}} \tag{25}$$

Where $s = \rho_s/\rho$

$$f(D_*) = \frac{0.30}{1+1.2D_*} + 0.055[1 - \exp\,(-0.02D_*] \tag{26}$$

The threshold velocity is lower for higher values of the particles diameter, therefore in a layered test the reference value for the critical velocity should be associated to the fine sand. If an experiment was performed with fine and coarse sand, and the coarse sand velocity was used, instead of the experiment being performed in the clear water regime it would occur in live bed regime.

Using Eq.(25) for the smaller sand, $d_{50} = 0.273mm$, was obtained a critical velocity of 0.24 m/s. The velocity was measured at 40% of the water depth in order to obtain a value closer to mean velocity of the flow according to Soulsby (1997).

When the velocity 0.24 m/s was tested, the experiment revealed to be in a live-bed regime (Figure 45). As there was a lot of sand being carried by the flow, it was necessary to determine a lower critical velocity, concluding that the equation established by Soulsby overestimates the critical velocity for the conditions that were used.

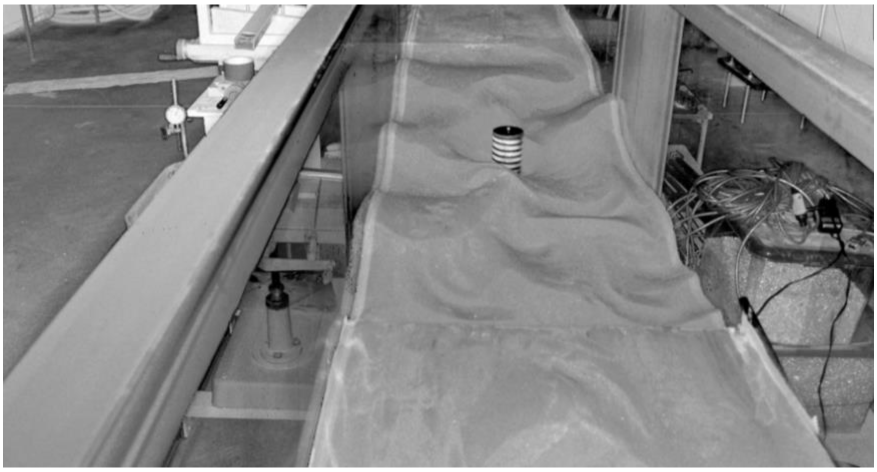

Figure 45. Live-bed regime in test with critical velocity equal to 0.24m/s

The average velocity value suitable to perform the experiments, according to Lencastre (1996) was 0.19 m/s.

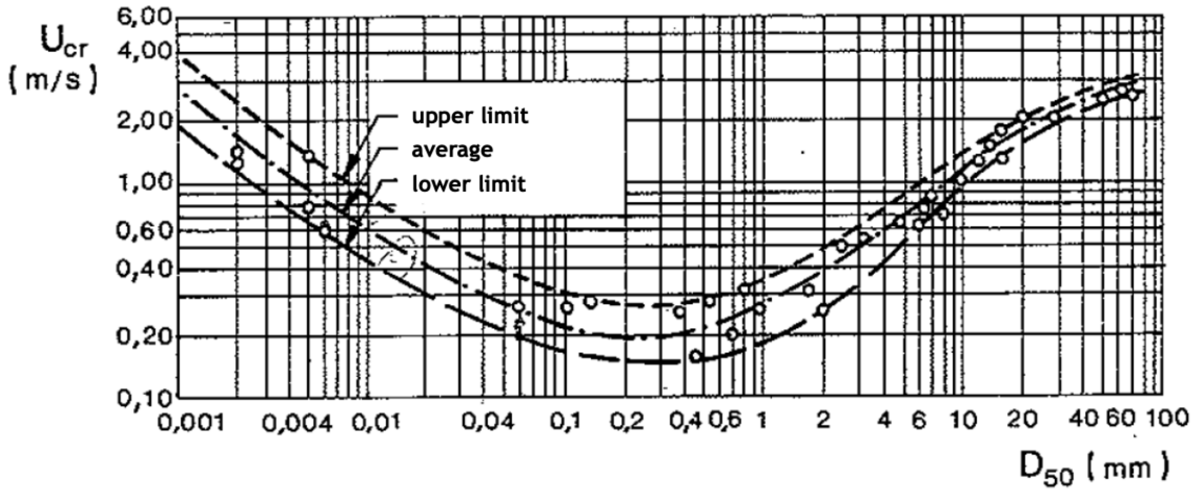

Figure 46. Average critical velocity as a function of the median diameter of sediments (Lencastre 1996)

3.5.3 TEST PLAN

The test plan consists of an initial scour test with the monopile foundation positioned on Fine Sand 1. Then the layered tests. In each test the upper layer had 3 cm. A scheme of the tests can be seen in Figure 47.

Table 7. Resume of the experiments performed

Test	h (m)	U_c (m/s)	D_p (m)	Re	Upper Layer	Lower Layer	Upper Layer Depth (cm)	Lower Layer Depth (cm)
1	0.15	0.19	0.05	9000	Fine Sand 1	-	20	-
2	0.15	0.19	0.05	9000	Fine Sand 1	Fine Sand 2	3	17
3	0.15	0.19	0.05	9000	Fine Sand 2	Fine Sand 1	3	17
4	0.15	0.19	0.05	9000	Coarse Sand	Fine Sand 1	3	17
5	0.15	0.19	0.05	9000	Fine Sand 1	Coarse Sand	3	17

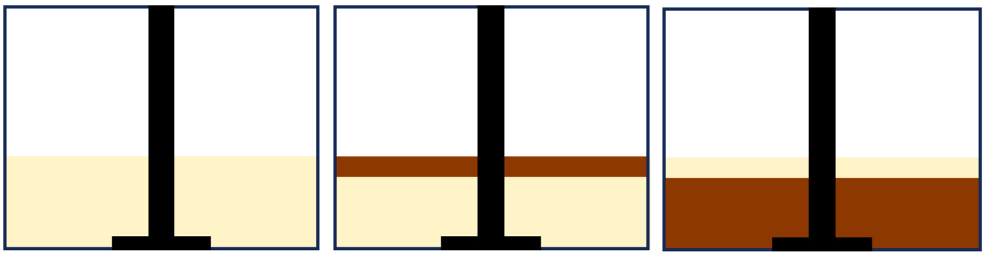

Figure 47. Scheme of the tests: one layer of sand (left); low layer of fine sand and upper of coarse sand (middle); lower layer of coarse sand and upper layer of fine sand (right)

3.5.4 MODEL EFFECTS CONSIDERATIONS

In the present study, model effects were carefully considered and mitigated to guarantee the reliability and accuracy of the experimental results. Some measures were taken in account to reduce their impact:

- The sand bed was always smoothed before the tests, to avoid the formation of ripples, so there is not sediment transport to the scour hole;
- Holes were drilled in the protection cover, which was placed at the beginning of each test while the channel was slowly filled so that the sand would not move, to avoid the vacuum effect and make it easier to lift;
- During the tests, the flume was filled and slowly emptied. This ensured that the sediment bed remained undisturbed before the start of each experiment and that after the end of the tests there were not changes in the scour hole to perform the final lasers;

- To guarantee that the boundary layer would be appropriately sized and that a completely rough boundary layer would exist along the entire length of the flume, the fake beds sections were covered and glued with sand on the top surfaces.

4 RESULTS, ANALYSIS AND DISCUSSION

4.1 EXPERIMENTAL GENERAL ANALYSIS

For each scour test, an individual compilation of the several data gathered was created, which can be seen in the Appendix. In this sub-section, an example of the information obtained in one test (Fine Sand 1) is presented. The scour tests were performed according to the procedures explained in 3.5.1. The experiments consisted in taking several measurements of the scour depth on the upstream side of the pile, in order to assess the scour development over time

Figure 48 presents the scour depth curve as a function of time, following an exponential law. It can be seen in the graphic the necessity of a higher rate of measurements in the initial moment of each experiment. In the first moments of scour development the higher rate of measurements taken is explained by the faster development of the scour depth in the initial phase than in the main and equilibrium phases.

The measurements presented in Figure 48 are the result of the direct reading in the pile ruler through the glass walls of the flume

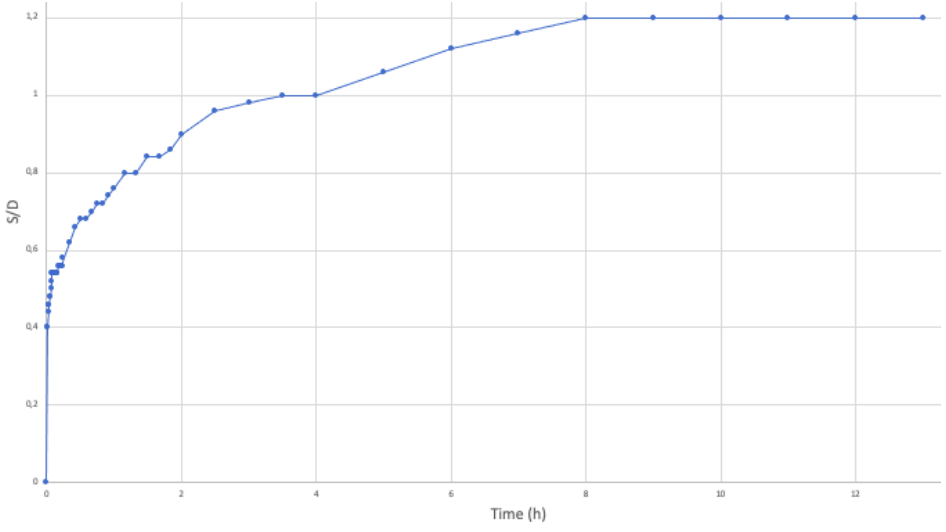

Figure 48. Scour depth curve vs time, Fine Sand 1

Table 8 presents the pile readings taken from this experiment.

Table 8. Pile readings for scour Fine Test 1

Time(min)	S (cm)	S/D	Time (min)	S(cm)	S/D
0	0.0	0.0	50	3.6	0.72
1	2.0	0.4	55	3.7	0.74
2	2.3	0.46	60	4.0	0.80
3	2.4	0.48	70	4.0	0.80
4	2.5	0.50	80	4.0	0.80
5	2.7	0.54	90	4.2	0.84
6	2.7	0.54	100	4.2	0.84
7	2.7	0.54	110	4.3	0.86
8	2.7	0.54	120	4.5	0.90
9	2.7	0.54	150	4.8	0.96
10	2.7	0.54	180	4.9	0.98
11	2.8	0.56	210	5.0	1.0
12	2.8	0.56	240	5.0	1.0
13	2.8	0.56	300	5.3	1.06
14	2.8	0.56	360	5.6	1.12
15	2.9	0.58	420	5.8	1.16
20	3.1	0.62	480	6.0	1.20
25	3.3	0.66	540	6.0	1.20
30	3.4	0.68	600	6.0	1.20
35	3.4	0.68	660	6.0	1.20
40	3.5	0.70	720	6.0	1.20
45	3.6	0.72	780	6.0	1.2

In the end of each experiment the scour hole presented a similar shape in every test, although the extent of the scour hole was different between them. Inside the scour hole was also noted that the maximum value for the scour depth was occurring on the upstream side of the pile, slightly misaligned with the flow.

4.2 EQUILIBRIUM SCOUR DEPTH ANALYSIS

In the present subchapter it can be found an in-depth analysis of the scour depth measurements for each test performed. The tests conditions and maximum scour depth are presented in Table 9. The scour depth vs time curves of each test can be found in the Annex.

Table 9. Table of scour results upstream the monopile

Test	Test Name	S (cm)	S/D
Fine Sand 1	FS1	6.00	1.20
Fine Sand 2 over Fine Sand 1	FS2_FS1	5.00	1.00
Fine Sand 1 over Fine Sand 2	FS1_FS2	5.30	1.06
Coarse Sand over Fine Sand 1	CS_FS1	4.50	0.90
Fine Sand 1 over Coarse Sand	FS1_CS	5.10	1.02

Figure 49 presents the scour depth curves for all the experiments, a uniform sand test and four layered tests. Regarding the scour depth curves it was expected that the Fine Sand 1 test, performed with only fine sand, would present the higher final scour depth, in agreement with other tests carried out previously by other authors like Ferradosa (2011).

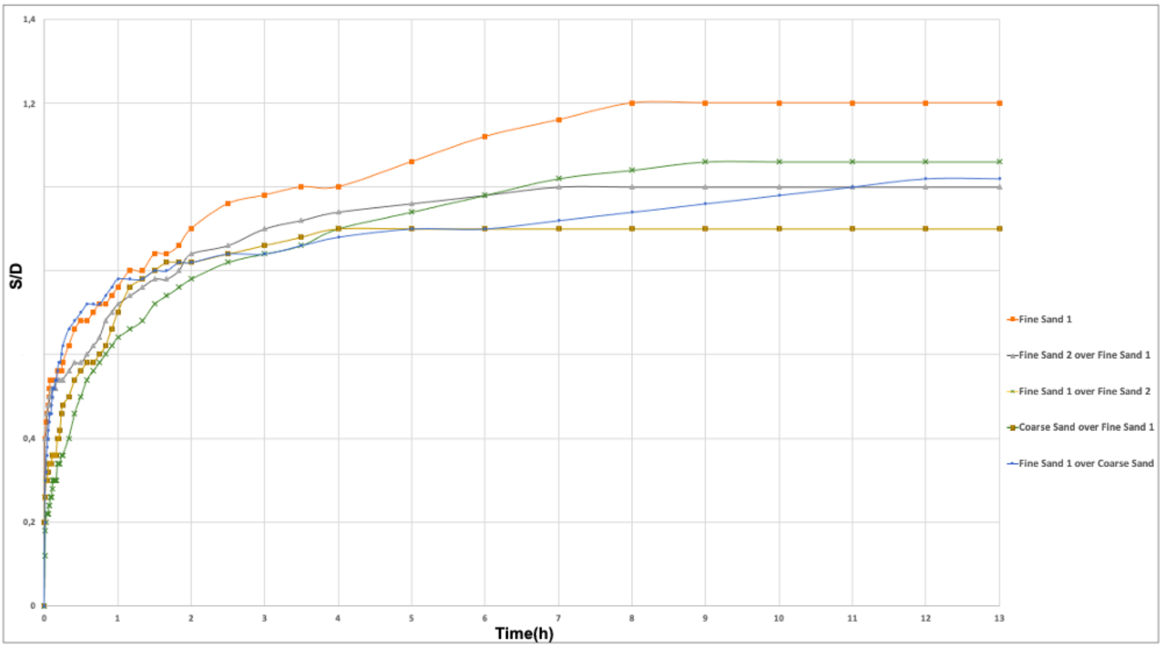

Figure 49. Scour depth vs. time curves

4.2.1 LAYERED SOILS: UNIFORMITY COEFFICIENT

When comparing the layered tests of Fine Sand 1 and Fine Sand 2, at the initial phase FS2_FS1 presented a higher scour depth until 6 hours of study reaching a S/D=1. This phenomenon is consistent with the literature considering Fine Sand 2 has a lower d_{50} being more prone to erosion. However, after 6 hours of testing there is an inversion in the curves. The scour depth from FS1_FS2 continues to increase and FS2_FS1 starts to stabilize.

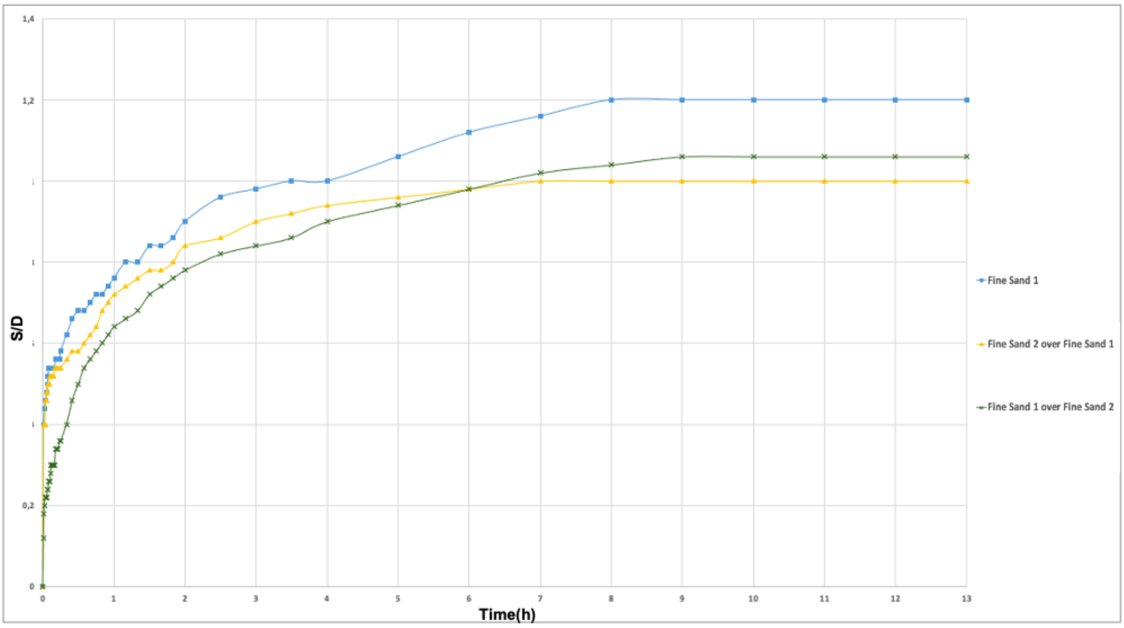

Figure 50. Scour depth vs Time for Fine Sand 1, Fine Sand 1 overlaying Fine Sand 2 and Fine Sand 2 overlaying Fine Sand 1

This phenomenon may be explained by differences in grading, while Fine Sand 1 is narrow graded with a uniformity coefficient of 1.8, Fine Sand 2 can be considered wide graded with a uniformity coefficient of 4.7. Having a lower uniformity means that the Fine Sand 1 particles are more similar in size (around d_{50}) while Fine Sand 2 presents particles ranging from 0.063-1 mm. Because Fine Sand 2 presents a higher value of σ_D (wider range of particles size) it may be more prone to the formation of an armouring layer. In the initial phase, when there is still a large quantity of the finer sediments in the Fine Sand 2 layer, scour development occurs "naturally", however, when the first sediments of the Fine Sand 2 layer are eroded and transported downstream, the larger sediments start to form an armouring layer around the pile and reaching stability earlier.

4.2.2 LAYERED SOILS: $\boldsymbol{d_{50}}$

Initially the curve from Fine Sand 1 overlaying Coarse Sand, the fine layer erodes quickly due to its low critical shear stress and the curve follows a similar trajectory to the Fine Sand 1(Figure 51). However, as the erosion reaches the coarse sand layer, close to 15 minutes, the coarser particles offer higher resisting forces due to their weight, slowing down the scour development.

When coarse sand is on top, the initial scour development is slower, indicating a slower rate of erosion. As erosion continues the underlaying fine sand is exposed at 50 minutes. The fine sand, having a lower critical shear stress, erodes faster. The combination of coarse sand and fine sand creates an interested behavior in the curve. As it can be seen in Ferradosa (2011), in mixed sand tests, the scour depth curve vs time does not have the usual scour depth vs time graphic. When the scour depth reaches the lower layers, the coarse and fine sand sediments mix with each other presenting different characteristics.

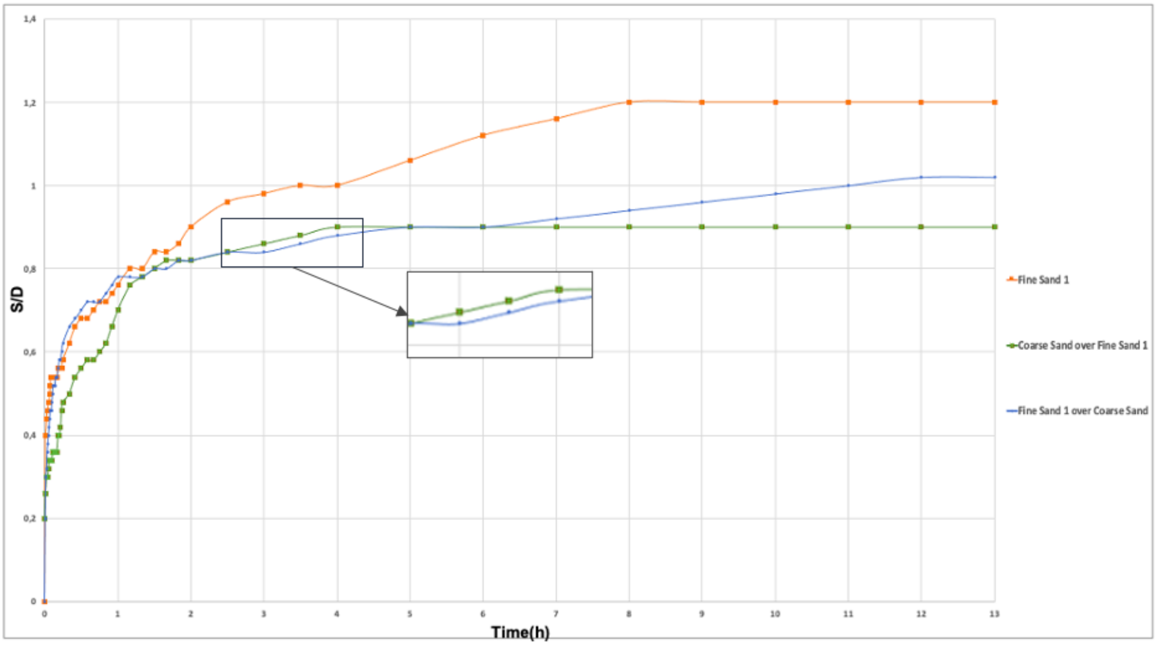

Figure 51. Inversion in the scour depth curves

After 6 hours of testing it can be seen another inversion in the curves, with the scour for a FS1_CS surpassing the scour for the CS_FS1. Scour in the CS_FS1 reached equilibrium at 4 hours, while the scour in FS1_CS continues to develop and did not reach equilibrium in the 13 hours of test.

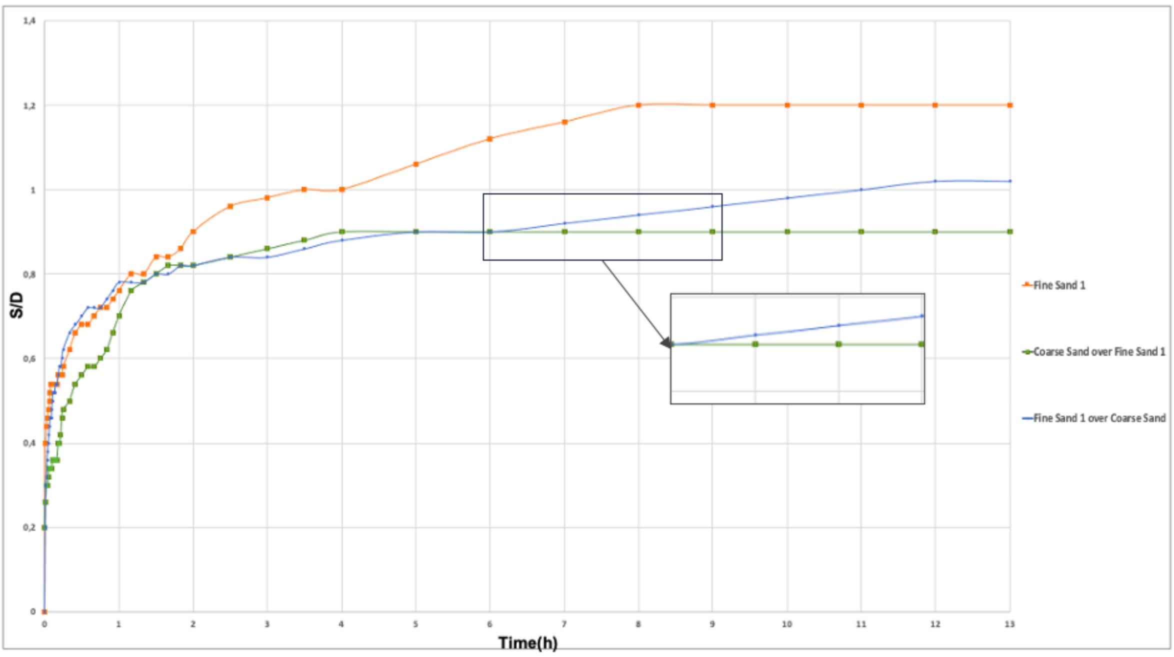

Figure 52. Inversion at the final phase

In the CS_FS1, even when the fine sand becomes exposed ,the coarse sand bigger particles may form an armoring layer , sheltering the fine sand underneath. Eventually the erosion reaches a point where the combination of coarser particles of the Coarse Sand with the Fine sand creates a stable configuration, resulting in a stabilization of the scour depth close to the 6 hours.

After 6 hours, in the FS1_CS test, the horseshoe and lee-wake vortices can still be strong enough to drag the underlaying Coarse Sand particles downstream, producing a continuous scour development. After the 13 hours of testing, the system did not reach the equilibrium and was still undergoing a significant erosion.

Ferradosa (2011) also performed tests with coarse and fine sand in layered configuration. The results obtained showed that when a Fine Sand was over a Coarse Sand the scour depth was lower than the tests with inverted layers. One explanation for the different results can be that the author chose to use the critical velocity for the fine sand, while in this dissertation it was chosen to keep the critical velocity below that for both sands.

4.3 SCOUR PATTERN ANALYSIS

In the present sub-chapter is found a qualitative analysis of scour and deposition patterns observed in the end of each test. This qualitative analysis was performed using the scour maps created with Cloud Compare software which are presented in Figure 53.

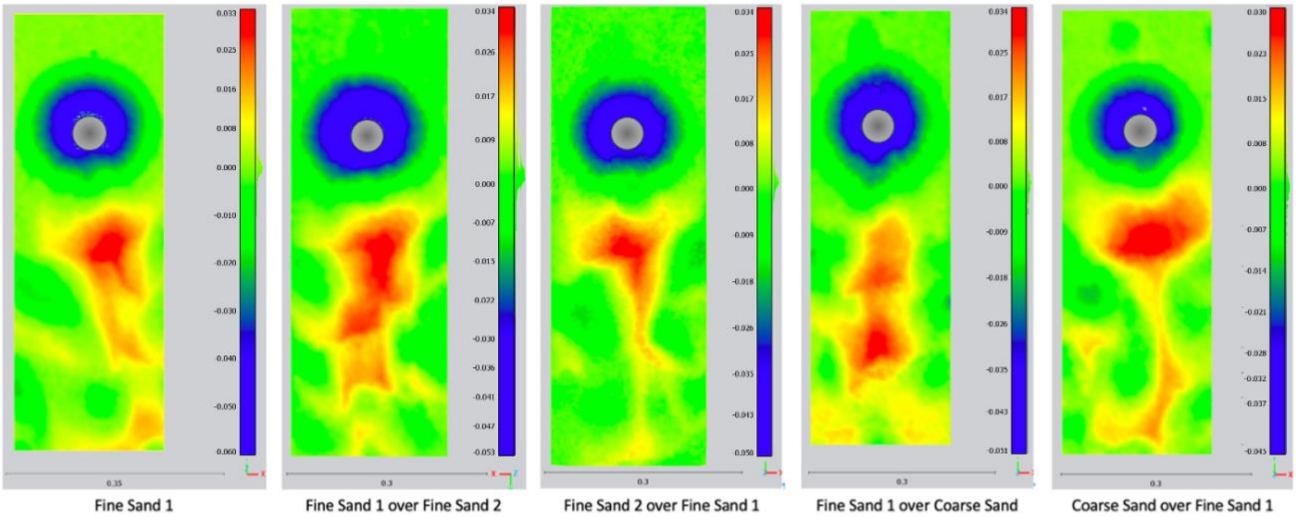

Figure 53. Monopile scour patterns (scale grading in meters)

Analyzing Figure 53 blue represents deeper scour zones, green represents less eroded areas and yellow/red shows deposition zones, with red indicating the highest value of deposition. In each test the upper part of the map represents upstream and the lower part the downstream, thus inferring the direction of the flow. All scour holes are generally circular and present symmetry around the pile.

Analyzing Fine Sand 1 scour map shows an eminent deposition zone downstream the pile with a highest value of 3.3 cm, highlighted in Figure 54.

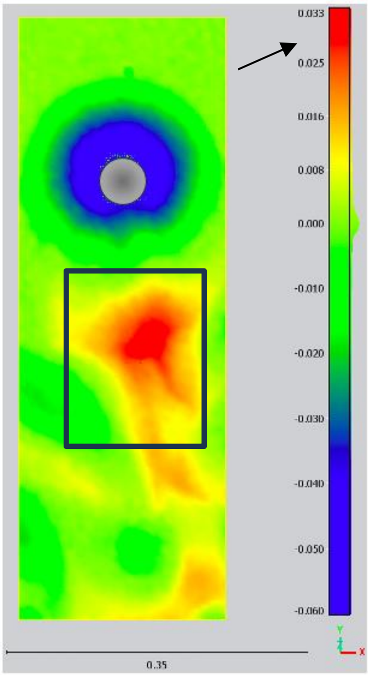

Figure 54. Fine Sand 1 scour pattern

The deposition occur after the pile extends in an elongated pattern, which can suggest that the eroded fine sand particles are carried and settled more downstream due to the flow. Can be seen some changes in the pattern downstream that may be due to the flow hitting the sand pile, undergoing a deviation and changing its deposition.

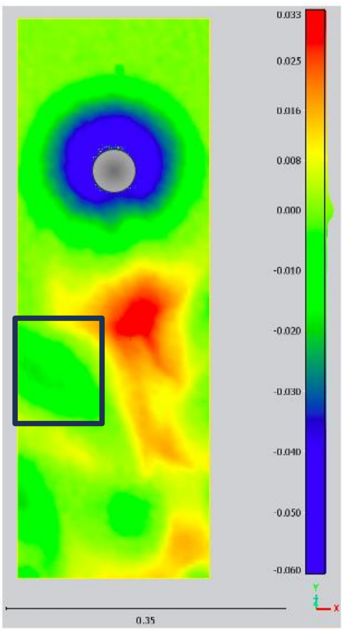

Figure 55. Fine Sand 1 changes in pattern

In Fine Sand 1 test the scour hole is circular and clearly defined. The central blue area indicates the higher depth around the pile. The scour hole appears symmetrical, although in the downstream part there is a small blemish that may be due to the way the laser scans were taken. The place where the final laser was placed was not high enough and, because of the sands deposition downstream, did not allow a clear image to be obtained on this side of the hole, creating a shadow.

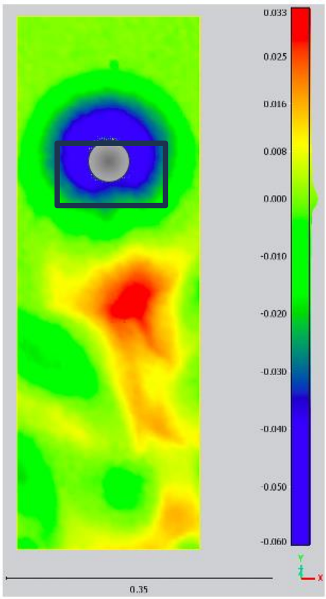

Figure 56. Fine Sand 1 laser's shadow

When the Fine Sand 1 is over Fine Sand 2 the deposition zone appears to be more concentrated and wider, indicating more sediment transport. The scour hole shows a larger blue area than the Fine Sand 1 test.

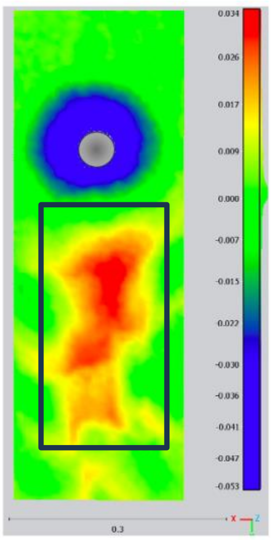

Figure 57. Fine Sand 1 over Fine Sand 2 scour map

Fine Sand 2 over Fine Sand 1 shows a smaller area of deposition than Fine Sand 1 overlaying Fine Sand 2, which can be derivate of the wider grader of Fine Sand 2. The bigger particles from the Fine Sand 2 did not had so much erosion as Fine Sand 1. In the test the scour pattern presents the most symmetry. The scour hole presents also the same problem explained before in the Fine Test 1.

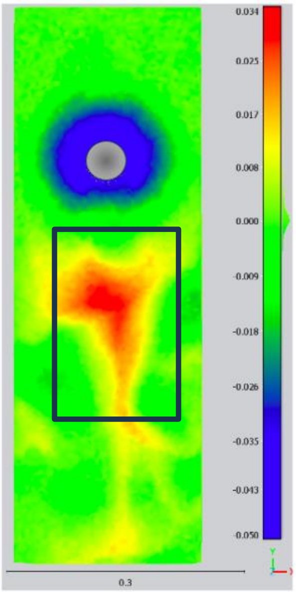

Figure 58. Fine Sand 2 over Fine Sand 1

In Fine Sand 1 over Coarse Sand test the sand begin to settle further away. The Coarse Sand underneath the fine sand affects the sediment transport, resulting in a more concentrated area. The scour pattern is also symmetric. Presents a circular scour hole but has a narrower area when compared with the test with Fine Sand 1 only.

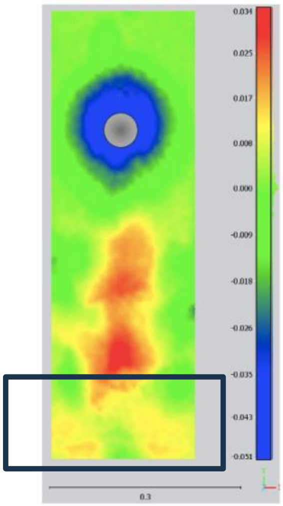

Figure 59. Fine Sand 1 over Coarse Sand

The last test, Coarse Sand over Fine Sand 1, presented less accumulation areas, having the smaller value of deposition sand of 3 cm. The deposition zone has a wider extent and more yellow zones, which may derive from when the scour depth reaches the bottom layer of fine sand it takes the sand and deposits it further down the flume. The smallest particles dispersed even more widely. Presents the scour hole with the smallest central blue area among the tests.

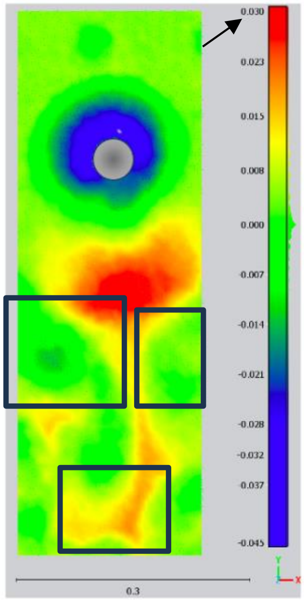

Figure 60. Coarse Sand over Fine Sand 1

It is important to refer that the symmetry of the scour holes indicates uniform flow conditions in the flume. Variations in the extent and depth on the scour holes are above all else due to the sediment properties and their interactions.

In general, fine sand layers result in more significant and extensive deposition zones. The presence of coarse sand reduces the overall deposition downstream due to its higher resistance to scour and lower transport.

4.4 PERPENDICULAR AND LONGITUDINAL PROFILES

4.4.1 LONGITUDINAL PROFILES

In order to analyze the development of the scour hole profile and the differences between the tests, 2D profiles of the scour hole upstream and downstream have been extracted from the Cloud Compare. The profiles of each test are presented in the Annex. In Figure 61 is presented all longitudinal profiles at the end of the performed tests.

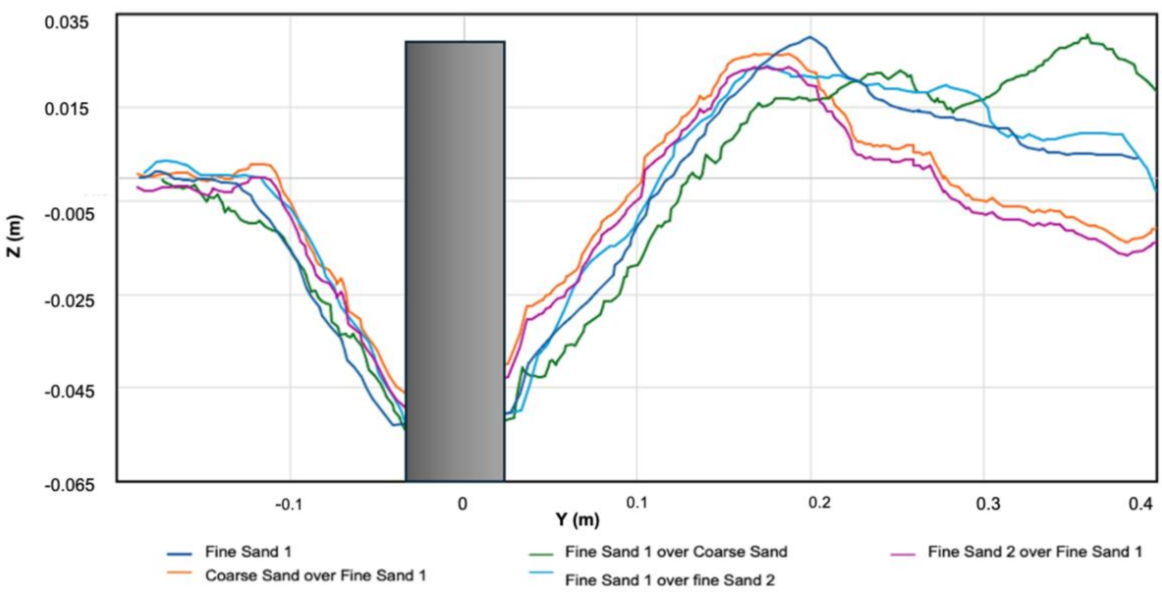

Figure 61. Longitudinal profiles for the experimental tests

By analyzing the graphic presented in Figure 61, the profiles show varying maximum scour depths depending on the sand configurations. The deepest scour occurs for Fine Sand 1 and the shallowest for Coarse Sand over Fine Sand 1.

The shape of the scour holes differs among the tests. The profiles where fine sand is overlaying show steeper and more defined scour holes when compared to the Coarse Sand over Fine Sand 1 test.

In Figure 61 can also be inferred the deposition zones downstream the pile, where the profiles rise more markedly. This is usually the area where the sediment settles because the flow slows down after crossing the pile. The extent and height of these downstream deposition zones vary with the sand type and layering, being more extensive for fine sand configurations, especially in the Fine Sand 1 test, where can be seen the highest peak.

Fine sand tends to be transported further, resulting in more pronounced deposition zones downstream of the pile. Coarse sand, being heavier and more resistant to be transport, shows less pronounced deposition zones, suggesting that it settles closer to the scour hole as it can be seen in the Coarse Sand over Fine Sand 1 curve.

In Figure 62 is presented a longitudinal profile of the Fine Sand 1test to show how the estimated slope angles have been calculated. The slope angles obtained are presented in Table 10.

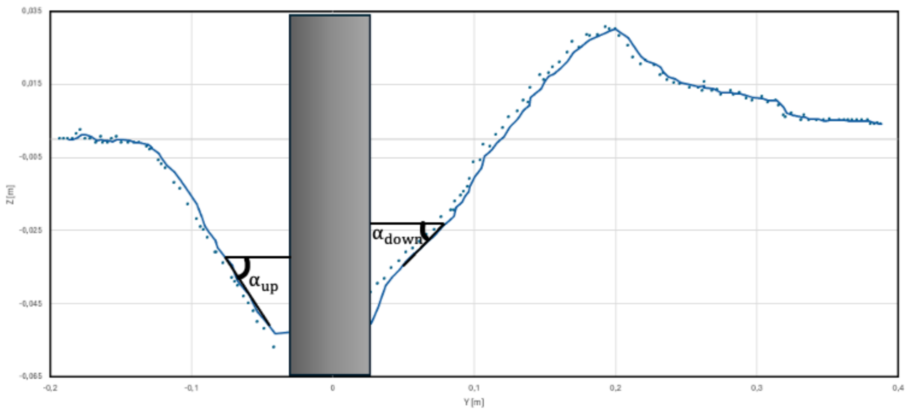

Figure 62. Fine Sand 1 longitudinal profile with fitted lines to estimate the upstream and downstream slope angles

Table 10. Estimated upstream and downstream scour hole slope angles

Test	Upstream (°)	Downstream (°)
Fine Sand 1	57	55
Fine Sand 1 over Fine Sand 2	60	65
Fine Sand 2 over Fine Sand 1	75	47
Coarse Sand over Fine Sand 1	49	50
Fine Sand 1 over Coarse Sand	64	50

For each case shown, the upstream scour hole slope is always slightly steeper than the downstream scour slope, except in the Fine Sand 1 over Fine Sand 2.

In Fine Sand 1 overlaying Fine Sand 2 test the upstream slope is lower than the downstream slope, being an exception, which can be due to varying grain sizes between the two sands, causing a different erosion process. The test with Fine Sand 2 over Fine Sand 1 had the highest slope angle, in line with what has already been said, being Fine Sand 2 more susceptible to erosion. In this three first tests an error in the final laser scans could have occurred. When the FARO Laser was placed in the position for reading the final profiles, the sand deposition zone just after the pile was not taken into account. Since the height of the laser was not high enough in relation to this area, the downstream zone of the erosion hole may not have been well represented. A scheme of the readings problem is shown in Figure 63. In the last two tests performed with the Coarse and Fine Sand 1 the laser has already been set higher so that there are no consequences for the laser scans readings.

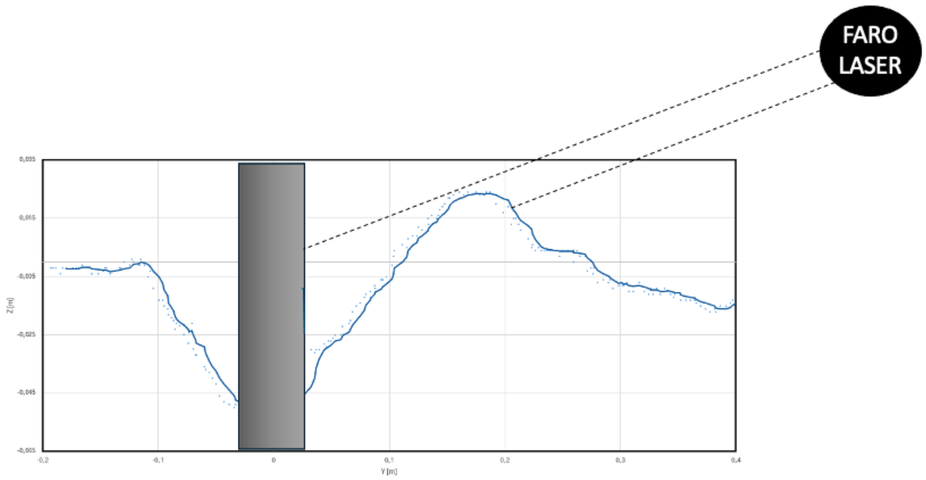

Figure 63. Laser scans performed

Coarse Sand over Fine sand presented the more similar slope angles upstream and downstream of the pile, suggesting a uniform scour hole. The upstream slope revealed to be less steep when compared to the test with only Fine Sand 1, indicating coarse sand has a higher resistance in the upstream.

The observation that the downstream slope angle is the same in the last two tests suggests similar erosion processes are occurring in both tests, despite the different sediment layering. An explanation can be the presence of bigger particles of the coarse sand that created an armor layer in both tests downstream.

According to DeVos (2008) the α_{down} should be approximately equal to $1/2\ \alpha_{up}$. These values were not verified in the tests results carried out. They may not have been obtained since the sand deposition area in the tests was very close to the scour hole area.

4.4.2 PERPENDICULAR PROFILE

By analyzing the perpendicular profiles of each scour test, the scour hole in the left side was consistently similar from the right side, showing some degree of symmetry. Figure 64 shows the perpendicular profile for the Fine Sand 1 test. In the Annex can be found the perpendicular profiles for the rest of the tests.

After the analysis of the perpendicular profiles of the tests, there is a flat zone near the pile. It can be explained by the capacity of the horseshoe vortices. First the horseshoe vortices have the strength to faster remove sediment, creating the scour hole depth. As the hole goes deeper the energy of the vortices dissipates. At some point, the horseshoe vortices have no longer strength to erode the bottom, leading to a flattening of the scour hole.

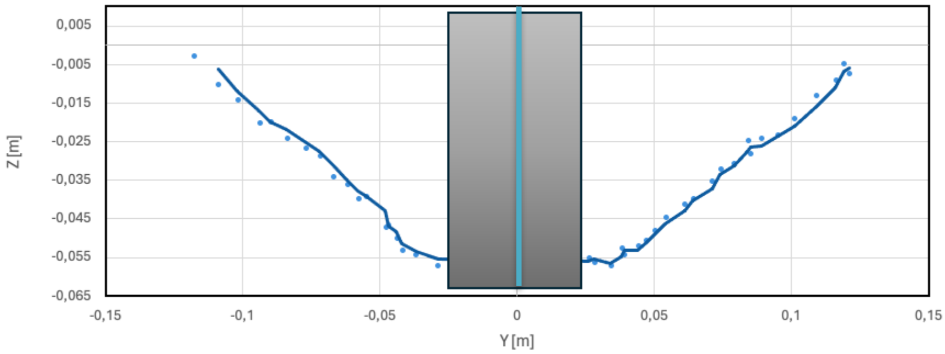

Figure 64. Fine Test 1 perpendicular profile

4.5 PREDICTING METHODS

The present subchapter provides the results obtained from the predicting methods and formulas presented in Chapter 2. These methods are limited for uniform sediments tests thus the following calculations were made for Fine Sand 1 test. The following table presents the results obtained by the scour depth predicting approaches.

Table 11. Scour depth values comparison between the experiments and the predicting theories, for a uniform pile (D_p=5cm)

Theoretical Approach	Predicted Value for Scour Depth (cm)	Experimental value for Scour Depth (cm)
	Fine Sand 1	Fine Sand 1
Melville and Coleman (2000)	11.64	
Breusers et al. (1977)	13.57	6
Froelich Design (1988)	9.31	

It is important to note that as expected none of the previous formulas predicted exactly the value of the scour depth verified in the experiments.

Table 12. Differences between the experimental results and the predicted values for scour depth in Fine Sand 1 test

Theoretical Approach	Scour depth difference between experimental and predicted values (%)
	Fine Sand 1
Melville and Coleman (2000)	94
Breusers et al. (1977)	126.17
Froelich Design (1988)	55

From the previous table is possible to state that the equation which provided the best overall results was the Froelich (1988).

The previously equations used to predict the scour depth are only applicable to situations in which the foundation soils are uniform. The inconsistent results obtained for Fine Sand 1 raise awareness that trying to predict the scour depth values for layered tests would lead to more unrealistic results. It is need in the equations a coefficient that takes into account the thickness of the top layer.

4.6 COMPARISON WITH PREVIOUS STUDIES

In the present sub-chapter is presented a comparative analysis with the studies discussed in Chapter 2. Table 13 presents the results obtained for the tests.

Table 13. S/D results comparison

	S/D Obtained		
Test	**Experimental Results**	**Ferradosa (2011)**	**Wang, Yuan et al. (2022)**
Fine Sand over Coarse Sand	1.02	1.6	0.5
Coarse Sand over Fine Sand	0.9	1.7	0.7

In the studies of Ferradosa (2011) and Wang, Yuan et al. (2022) a higher S/D value was obtained when the coarse sand was overlaying fine sand, different from the experimental results obtained in the present study.

The difference in Ferradosa (2011) may be due to the fact that the author used a critical velocity for the fine sand. This may have caused the experiment of Fine Sand over Coarse Sand to take place in a live-bed regime, causing the formation of ripples which, with the flow, led to sediments being deposited in the scour hole, reducing the depth of the scour. The curves obtained in the study can be observed in Figure 65.

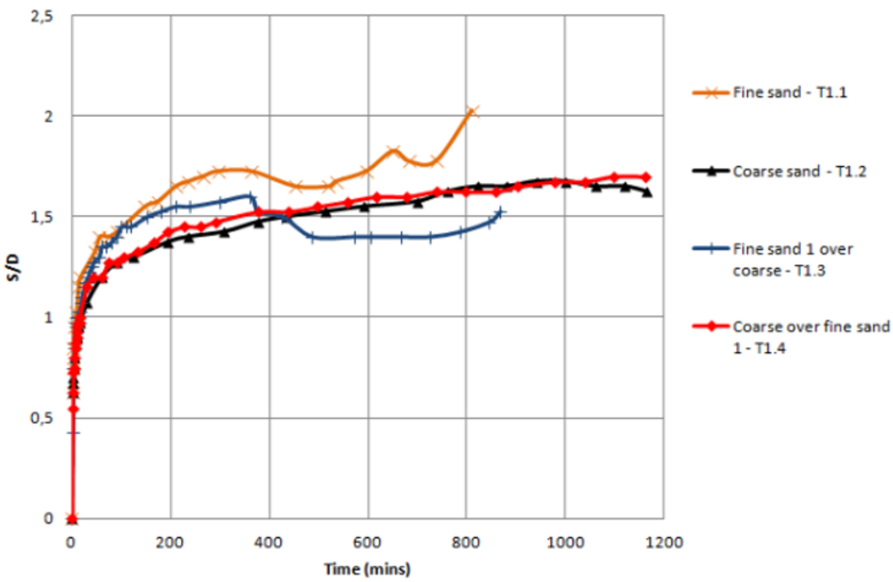

Figure 65. Scour depth vs time (Ferradosa (2011))

In the study of Wang, Yuan et al. (2022) the author also presents a higher scour for the Coarse Sand over Fine Sand. In Figure 66 is presented the results from the author.

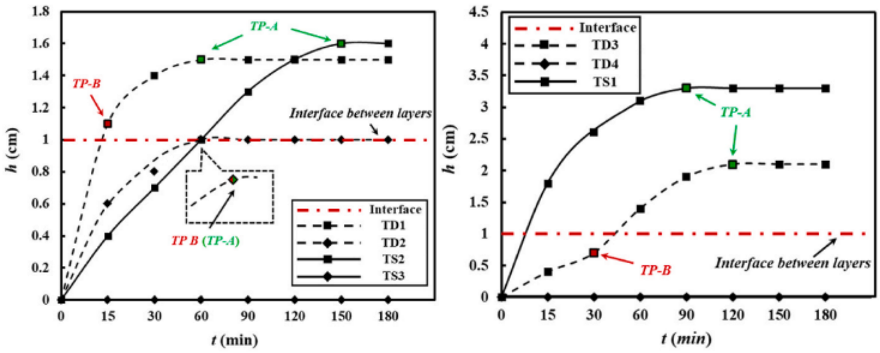

Figure 66. Results from Wang, Yuan et al. (2022) : TD1 represents Fine Sand over Coarse Sand (left); TD2 represents Coarse Sand over Fine Sand (right)

As it can be seen in the previous figure the author stops the test after 3 hours of testing. At this point TD3 the test with Coarse sand overlying, presented a higher value of scour than TD1, where fine sand is overlying. Because it seems that the equilibrium is reached the author stops the test.

In the experimental tests of the present dissertation, at the same time interval of 3 hours, the same behavior of the curves was verified, as it can be seen in Figure 67.

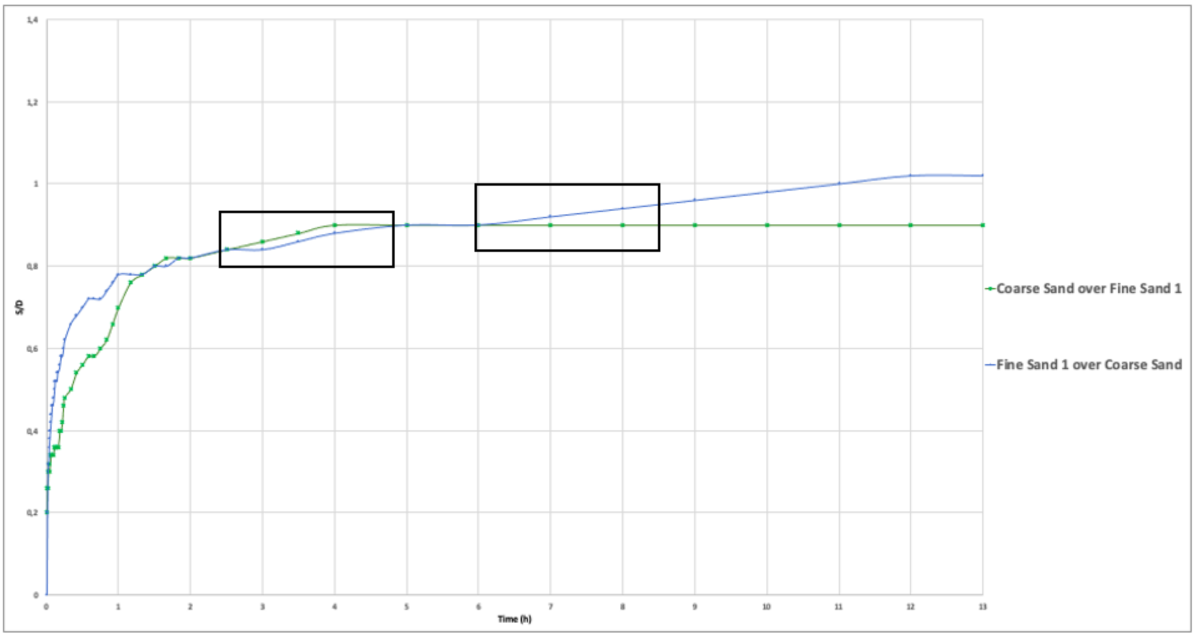

Figure 67. Scour depth curves for Coarse and Fine Sand 1 layered tests

However, the test was only stopped after 13 hours. After 6 hours the curves reverse and the fine sand overlying presents a higher scour depth than the coarse sand overlying. The time of the test was an important variable because if the test was stopped after 3 hours the results would be completely different. If Wang, Yuan et al. (2022) had continued the tests, perhaps the curves would have turned too.

5 CONCLUSIONS AND FUTURE WORK

5.1 CONCLUSIONS

The present study allowed a deeper analysis and knowledge regarding the several mechanisms that lead to scour phenomenon around complex foundations. Among the several variables that tend to have an impact on scour a special focus was given to the foundation soil's influence upon the scour process, namely, regarding monopile foundations founded on layered soil morphology.

This research consisted in analyzing the several scour parameters such as the scour depth, the scour hole extent and general shape of the sour depth vs. time curves for five experimental tests. The first test performed only with Fine Sand 1, which allowed for a comparison with further tests. Next were performed layered bed tests, with Fine Sand 1 over Fine Sand 2, Fine Sand 2 over Fine Sand 1, Coarse Sand over Fine Sand 1 and Fine Sand 1 over Coarse Sand.

The experiments performed provided the data discussed in chapter 4 that allowed the drawing of the following conclusions:

- The equation presented by Soulsby (1997) overestimates the critical current speed, showing results that are higher than those that actually occur;
- Fine sands configurations presented the higher scour depths, with Fine Sand 1 test showing the highest scour depth;
- The uniformity coefficient of the sands is an important parameter, because the Fine Sand 2 overlaying Fine Sand 1 test, showed a lower scour depth than the Fine Sand 1 test, proving that Fine Sand 2, despite having a lower percentage of bigger particles, it was enough to influence the process and cause a decrease in the scour depth;
- The presence of coarse sand significantly reduces scour depth. Both configurations with coarse sand resulted in lower scour depth. The coarse sand may cause armour layer effect, reducing the extent of scour;
- The scour holes were wider when Fine Sand 1 was the top layer;
- The obtained results for the Fine Sand 1 overlaying Coarse Sand were not in agreement with the results tested by Ferradosa (2011) and Wang, Yuan et al. (2022). The present dissertation obtained a higher scour depth with this configuration than with Coarse Sand overlaying Fine Sand 1, while the authors obtained more scour when Coarse Sand was the overlying layer. This

can be explained by the use of a critical velocity in the experiments by the first author, while in this dissertation the velocity was not critical for any of the sands. For the second author, the fact that he opted for only 3 hours of testing influenced the results obtained;

- Regarding the methodologies described before to predict scour depth, Froelich (1988) theory provided the best approximation to the experimental values, with an overestimation of 55%.

The data provided through the present study was important in order develop a solid contribution to scour research around monopile foundations. The goal of this dissertation was to provide a qualitative and quantitative analysis regarding uniform and layered sand-beds, exposed to a unidirectional current which will enable future research efforts in larger-scale research.

5.2 FUTURE WORK

Some suggestions are made in order to provide some guidelines for further investigation:

- Try the same experiments but with different critical velocities for each sand tested, in order to better understand the influence of clear-water or live-bed regime;
- Have more experiments to understand the influence of the thickness of the overlying layer and its influence;
- Increase the number of layers used in the tests and understand how their structure affects the scour process;
- It is also important to study more about the mixed sand beds, because they clearly have an influence, since sand mixing can also occur in layered tests.

6 SUSTAINBLE DEVELOPMENT GOALS ALIGMENT

A plan of action covering a wide range of social, environmental, and technological issues, from poverty reduction, health for all, infrastructure development, education, and gender equality, to the sustainable use of oceans, energy, water, and sanitation, the 17 Sustainable Development Goals (SDG) were formulated to increase awareness of the various facets of sustainability. Engineering is relevant to all 17 goals, and engineering is necessary for each goal to be accomplished. In order to overcome the issues of climate change, population expansion, and urbanization while maintaining sustainable development, creative engineering and technological solutions will be necessary (UNESCO 2021).The present dissertation addresses the following Sustainable Development Goals: 7, 11, 13, and 14.

The SDG 7 ensure access to affordable, reliable, sustainable and modern energy for all. The SDG 11 has the goal to make cities and human settlements inclusive, safe, resilient and sustainable. According to the SDG 13 is urgent to take action to combat climate change and its impacts. Finally, the SDG 14 agrees to conserve and sustainably use the oceans, seas and marine resources for sustainable development. Each goal has its specific targets and indicators to measure the progress.

In order to know how the realization of this dissertation aligns with the SDGs and how it can maximize its impact, for each SDG its goal, contribution of the study and respective indicators were described.

Table 14 presents an assessment of the contributions of the present research for the achievements of the goals defined by the United Nations in 2015.

Table 14. Sustainable Development Goals Assessment

SDG	Target	Contributions of the Dissertation	Performance indicators and Metrics
7	**7.2**	Contributes to the advancement off offshore wind energy, a valuable component of renewable energy sources. By improving the understanding of scour, helps enhance the efficiency and reliability of offshore wind farms, supporting the goal of increasing the share of renewable energy	>6 million kWh of electricity per year
11	**11.3**	The promotion and development of offshore wind energy support the goal of sustainable communities by providing clean energy solutions. This contributes to the sustainability of cities and communities by reducing dependence on non-renewable energy sources.	1 MWh of wind energy avoids 75 tons of carbon dioxide emissions on average
13	**13.2.2**	Offshore wind energy plays a clean alternative to fossil fuels. By addressing the scour phenomenon, the research contributes to combat climate change and mitigate its impacts	1 MWh of wind energy avoids 75 tons of carbon dioxide emissions on average
14	**14.2**	Properly managed offshore wind installations can coexist with marine life, minimizing the impact on seabed habitats and contributing to the conservation and sustainable use of ocean resources.	A monopile foundation can create new habitat for marine life

BIBLIOGRAPHY.

Breusers, H. N. C., G. Nicollet and H. W. Shen (1977). "Local Scour Around Cylindrical Piers." Journal of Hydraulic Research **15**: 211-252.

Breusers, H. N. C. and A. J. Raudkivi (1991). Scouring Hydraulic Structures Design Manual

Breusers, H. N. C. and A. J. Raudkivi (1991). Scouring-Hydraulic Structures Design Manual Series, Vol 2.

Chambel, J. (2019). Analysis of Long-Term Damage of Offshore Wind Turbine Foundations. Master, FEUP.

Collins, C. (2017). Development and application of a computational model for scour around offshore wind turbine foundation. Doctor of Philosophy, University of Hull.

Desalegn, B., D. Gebeyehu, B. Tamrat, T. Tadiwose and A. Lata (2023). "Onshore versus offshore wind power trends and recent study pratices in modeling of wind turbines life-cycle impact assessments." Science Direct.

DeVos, L. (2008). Optimisation of Scour Protection Design for Monopiles and Quantification of Wave Run-Up. PhD, Ghent University.

Engineering, E. (2023). Guide to Offshore Wind Foundations. Empire Engineering.

Ferradosa, T. (2011). Scour Around Marine Foundations In Mixed And Layered Sediments Master, Porto.

Ferradosa, T. (2018). Reability Analysis Applied To The Optimization Of Dynamic Scour Protections For Offshore Windfarm Foundation, FEUP.

Froelich, D. C. (1988). "Analysis of Onsite Measurements of Scour at Piers." Hydraulic Engineering: 534-539.

Frostick, L. E., S. J. McLelland and T. G. Mercer (2011). Users Guide to Physical Modelling and Experimentation.

Hauwere, N. D. (2016). "Marineregions.maps." from https://www.marineregions.org/maps.php?album=3747&pic=115812.

Hoffmans, G. J. C. M. and H. L. Verheij (2021). Scour Manual- Current-Related Erosion.

Hughes, S. A. (1993). Physical Models and Laboratory Techniques in Coastal Engineering.

IRENA (2019). Future of Wind: Deployment, investment, technology, grid integration and socio-economic aspects.

IRENA (2023). Offshore Wind Energy-Patent insight report.

Lencastre, A. (1996). Hidráulica Geral.

Liu, Z. (2001). Sediment Transport. Aalborg University.

Matutano, C. (2013). Caracterización de los sistemas de protección basados en materiales naturales destinados al control de la socavación en obras marítimas presentes en instalaciones eólicas marinas, Caracterización de los sistemas de protección basados en materiales naturales destinados al control de la socavación en obras marítimas presentes en instalaciones eólicas marinas.

Melville, B. (2008). "THE PHYSICS OF LOCAL SCOUR AT BRIDGE PIERS ".

Melville, B. and A. J. Raudkivi (1977). "Flow Characteristics in Local Scour at Bridge Piers." Journal of Hydraulic Engineering.

Melville, B. and J. Sutherland (1988). "Design Method for Local Scour at Bridge Piers." Journal of Hydraulic Engineering.

Melville, B. W. and Y.-M. Chiew (1999). Time Scale for Local Scour at Bridge Piers.

Melville, B. W. and S. E. Coleman (2000). Bridge Scour, Water Resources Publications.

Menéndez-Vicente, C., S. López-Querol, S. Bhattacharya and R. SImons (2023). "Numerical Study on the Effects of Scour on Monopile Foundations for Offshore WInd Turbines: The case of Robin Rigg wind farm." Elsevier.

Miranda, F. (2022). Experimentall Study On Scour Around Foundations For Marine Energy Harvesting Technologies In Complex Soils. Master, FEUP.

NORTEK (2018). The comprehensive Manual for Velocimeters.

Porter, K., J. M. Harris, R. R. Simons and T. F. Ferradosa (2013). A laboratory study of scour in mixed and layered sand beds.

Porter, K. E. (2016). Seabed scour around marine structures in mixed and layered sediments University College London.

Rijn, L. C. v. (1993). Principles of Sediment Transport in Rivers, Estuaries and Coastal Seas.

Secção de Hidráulica, R. H. e. A. "Laboratório de Hidráulica."

Shields, A. (1936). Application of similarity principles and turbulence research to bed-load movement. PhD.

Soulsby, R. (1997). Dynamic of marine sands- A manual for practical applications, Thomas Telford Publication.

Soulsby, R. (1997). Dynamics of Marine Sands: A manual for practical application, Thomas Telford.

Sumer, B. M., N. Christiansen and J. Fredsoe (1992). Time Scale Of Scour Around A Vertical Pile. The Second International Offshore and Polar Engineering Conference.

Sumer, B. M. and J. Fredsøe (1997). Hydrodynamics Around Cylindrical Structures.

UNESCO (2021). Engineering for Sustainable Development.

Vindenesa, H., K. A. Orvika, H. Søilandb and H. Wehdeb (2018). "Analysis of tidal currents in the North Sea from shipboard acoustic Doppler current profiler data." Continental Shelf Research.

Wang, C., Y. Yuan, F. Liang and J. Tao (2022). "Experimental investigation of local scour around cylindrical pile foundations in a double-layered sediment under current flow." Ocean Engineering.

Webber, N. B. (1971). Fluid Mechanics for Civil Engineers. London.

WenGang, Q. and G. FuPing (2014). Equilibrium scour depth at offshore monopile foundation in combined waves and current SCIENCE CHINA.

Whitehouse, R. (1998). Scour at Marine Structures. London.

WindEurope. (2022). "Offshore Wind Energy."

WindEurope (2023). Wind Energy in Europe-2023 Statistics and the outlook for 2024-2030. R. O’Sullivan.

ANNEX

A.1. FINE SAND 1 RESULTS

Time(min)	S (cm)	S/D	Time (min)	S(cm)	S/D
0	0.0	0.0	50	3.6	0.72
1	2.0	0.4	55	3.7	0.74
2	2.3	0.46	60	4.0	0.80
3	2.4	0.48	70	4.0	0.80
4	2.5	0.50	80	4.0	0.80
5	2.7	0.54	90	4.2	0.84
6	2.7	0.54	100	4.2	0.84
7	2.7	0.54	110	4.3	0.86
8	2.7	0.54	120	4.5	0.90
9	2.7	0.54	150	4.8	0.96
10	2.7	0.54	180	4.9	0.98
11	2.8	0.56	210	5.0	1.0
12	2.8	0.56	240	5.0	1.0
13	2.8	0.56	300	5.3	1.06
14	2.8	0.56	360	5.6	1.12
15	2.9	0.58	420	5.8	1.16
20	3.1	0.62	480	6.0	1.20
25	3.3	0.66	540	6.0	1.20
30	3.4	0.68	600	6.0	1.20
35	3.4	0.68	660	6.0	1.20
40	3.5	0.70	720	6.0	1.20
45	3.6	0.72	780	6.0	1.2

Table A.1 1. Pile readings Fine Sand 1

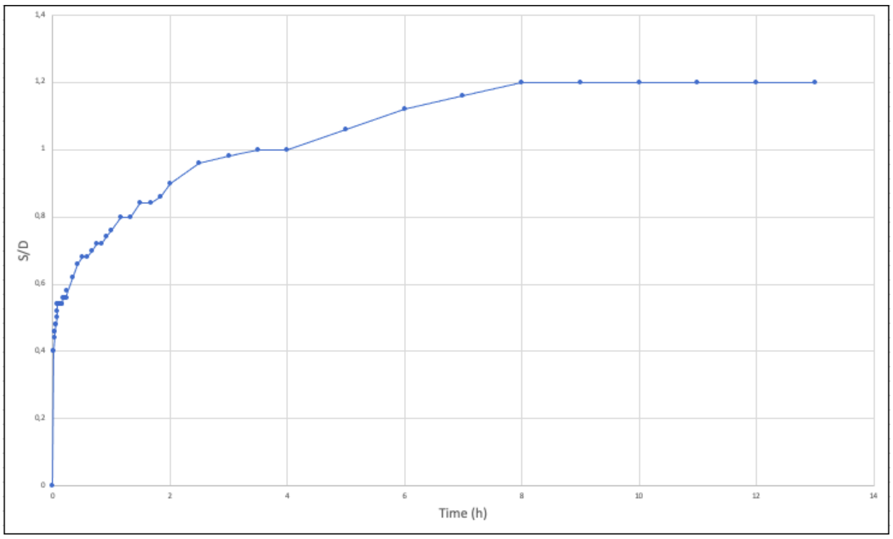

Figure A.1 1. Scour depth vs time for Fine Sand 1

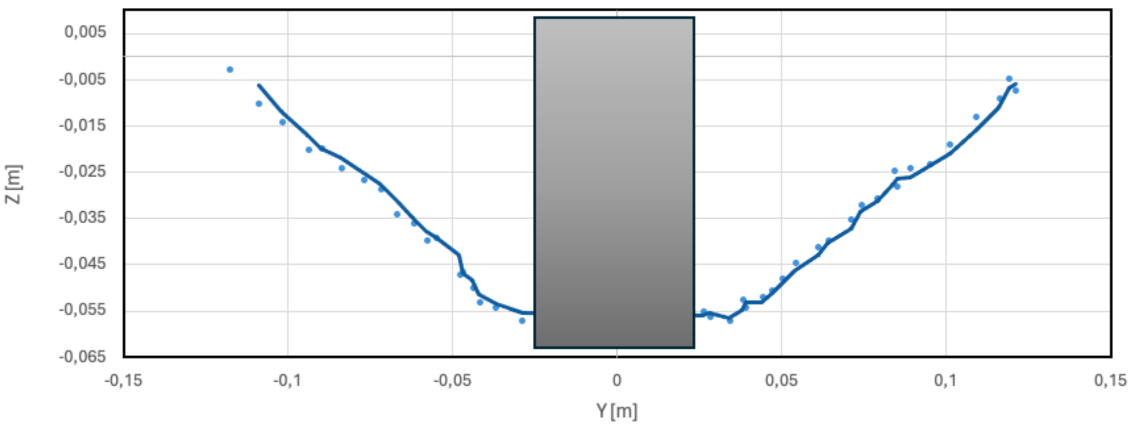

Figure A.1 2. Perpendicular profile of Fine Sand 1

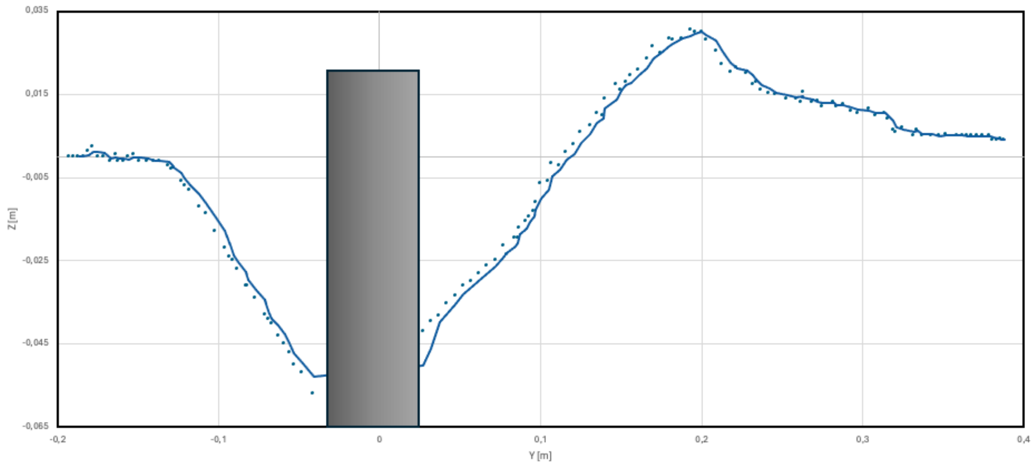

Figure A.1 3. Longitudinal profile of Fine Sand 1

A.2. FINE SAND 2 OVER FINE SAND 1 RESULTS

Time(min)	S (cm)	S/D	Time (min)	S(cm)	S/D
0	0.0	0	**50**	3.4	0.68
1	2.0	0.4	**55**	3.5	0.70
2	2.0	0.4	**60**	3.6	0.72
3	2.3	0.46	**70**	3.7	0.74
4	2.4	0.48	**80**	3.8	0.76
5	2.5	0.50	**90**	3.9	0.78
6	2.6	0.52	**100**	3.9	0.78
7	2.6	0.52	**110**	4.0	0.80
8	2.6	0.52	**120**	4.2	0.84
9	2.6	0.52	**150**	4.3	0.86
10	2.7	0.54	**180**	4.5	0.90
11	2.7	0.54	**210**	4.6	0.92
12	2.7	0.54	**240**	4.7	0.94
13	2.7	0.54	**300**	4.8	0.96
14	2.7	0.54	**360**	4.9	0.98
15	2.7	0.54	**420**	5.0	1.0
20	2.8	0.56	**480**	5.0	1.0
25	2.9	0.58	**540**	5.0	1.0
30	2.9	0.58	**600**	5.0	1.0
35	3.0	0.50	**660**	5.0	1.0
40	3.1	0.62	**720**	5.0	1.0
45	3.2	0.64	**780**	5.0	1.0

Figure A.2 1. Pile readings

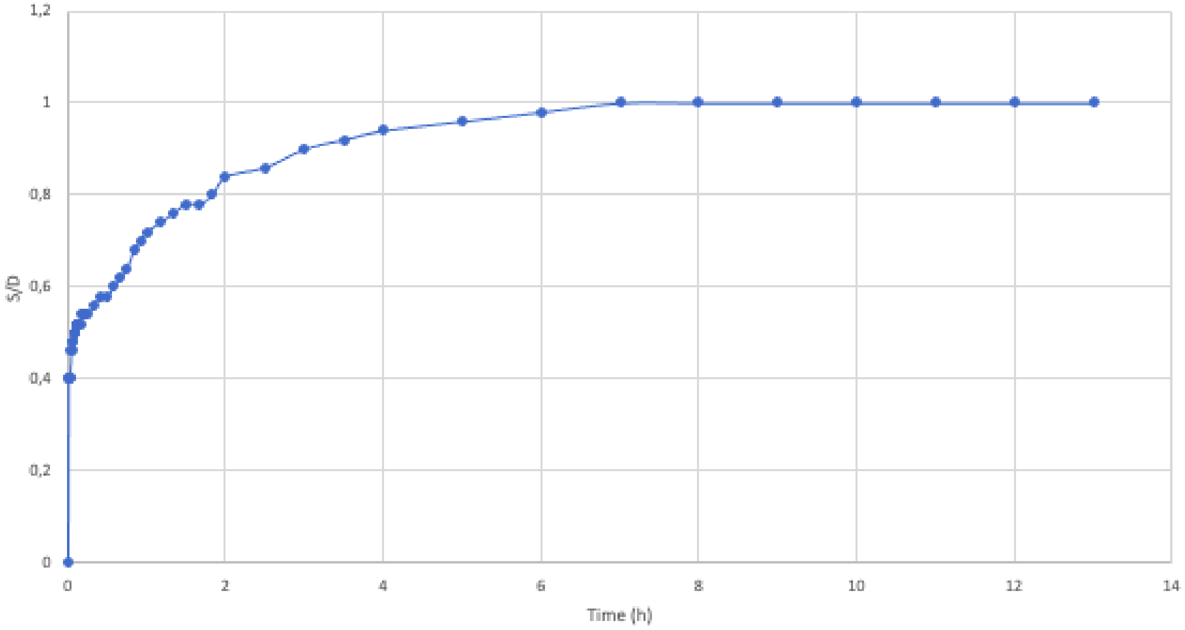

Table A.2 1. Scour depth vs time for Fine Sand 2 over Fine sand 1

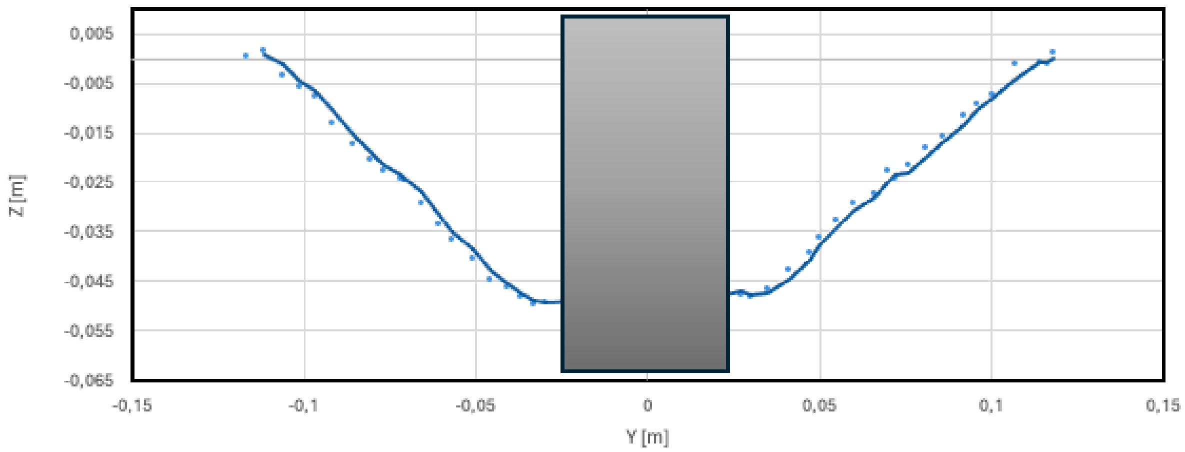

Figure A.2 2. Perpendicular profile for Fine Sand 2 over Fine Sand 1 test

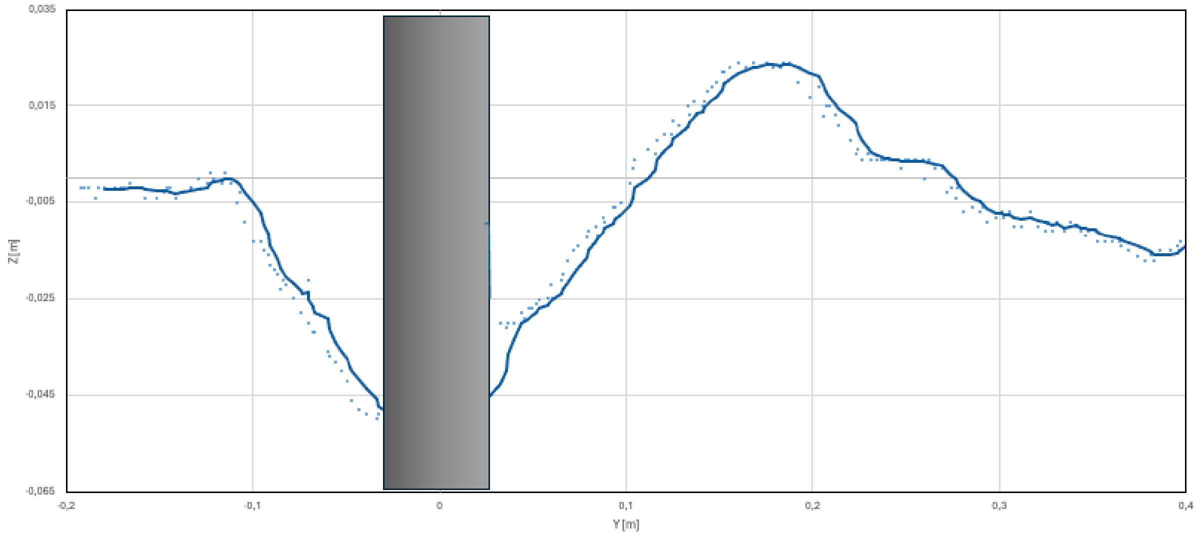

Figure A.2 3. Longitudinal profile for Fine Sand 2 over Fine Sand 1

A.3. FINE SAND 1 OVER FINE SAND 2 RESULTS

Time(min)	S (cm)	S/D	Time (min)	S(cm)	S/D
0	0	0	**50**	3	0.60
1	1	0.20	**55**	3.1	0.62
2	1.1	0.22	**60**	3.2	0.64
3	1.1	0.22	**70**	3.3	0.66
4	1.2	0.24	**80**	3.4	0.68
5	1.3	0.26	**90**	3.6	0.72
6	1.3	0.26	**100**	3.7	0.74
7	1.5	0.30	**110**	3.8	0.76
8	1.5	0.30	**120**	3.9	0.78
9	1.5	0.30	**150**	4.1	0.82
10	1.5	0.30	**180**	4.2	0.84
11	1.7	0.34	**210**	4.3	0.86
12	1.7	0.34	**240**	4.3	0.86
13	1.7	0.34	**300**	4.5	0.90
14	1.8	0.36	**360**	4.7	0.94
15	1.8	0.36	**420**	4.9	0.98
20	2	0.40	**480**	5.1	1.02
25	2.3	0.46	**540**	5.2	1.04
30	2.5	0.50	**600**	5.3	1.06
35	2.7	0.54	**660**	5.3	1.06
40	2.8	0.56	**720**	5.3	1.06
45	2.9	0.58	**780**	5.3	1.06

Table A.3 1. Pile readings for Fine Sand 1 over Fine Sand 2

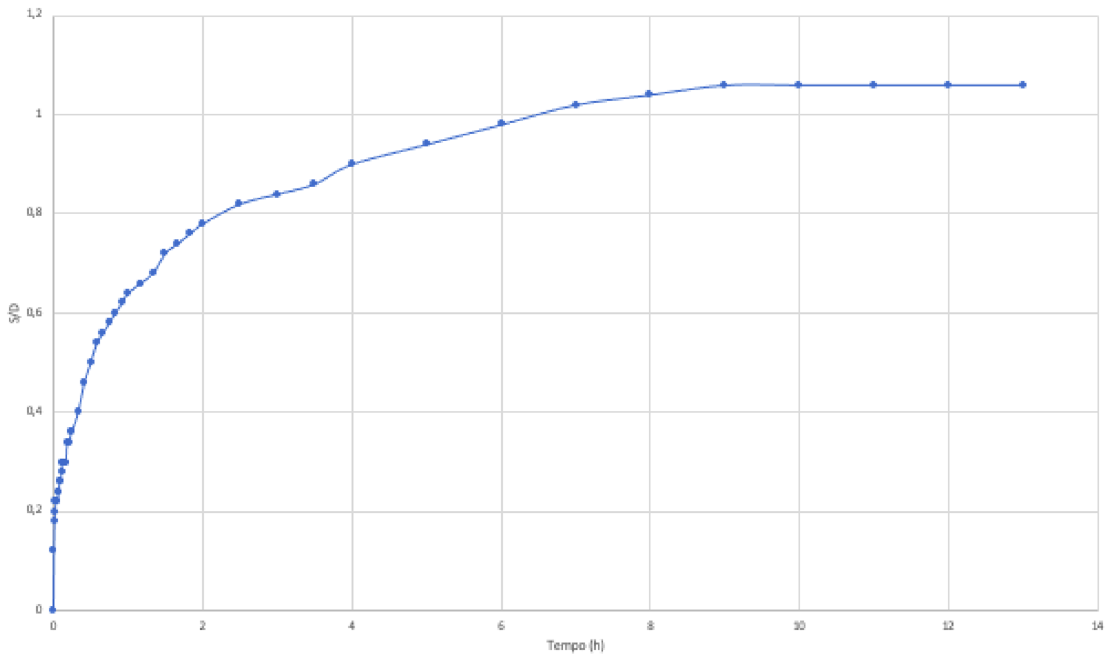

Figure A.3 1. Scour depth vs time for Fine Sand 1 over Fine Sand 2 test

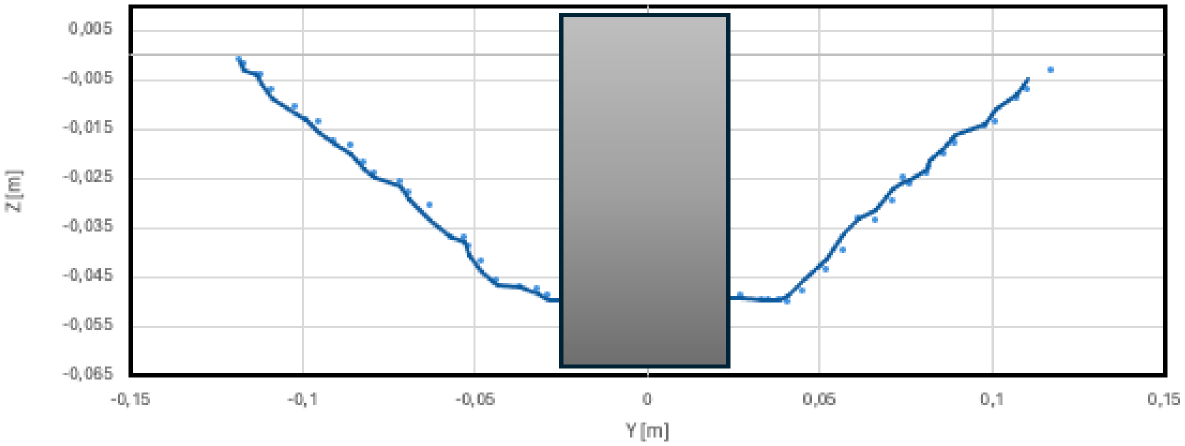

Figure A.3 2. Perpendicular profile for Fine Sand 1 over Fine Sand 2

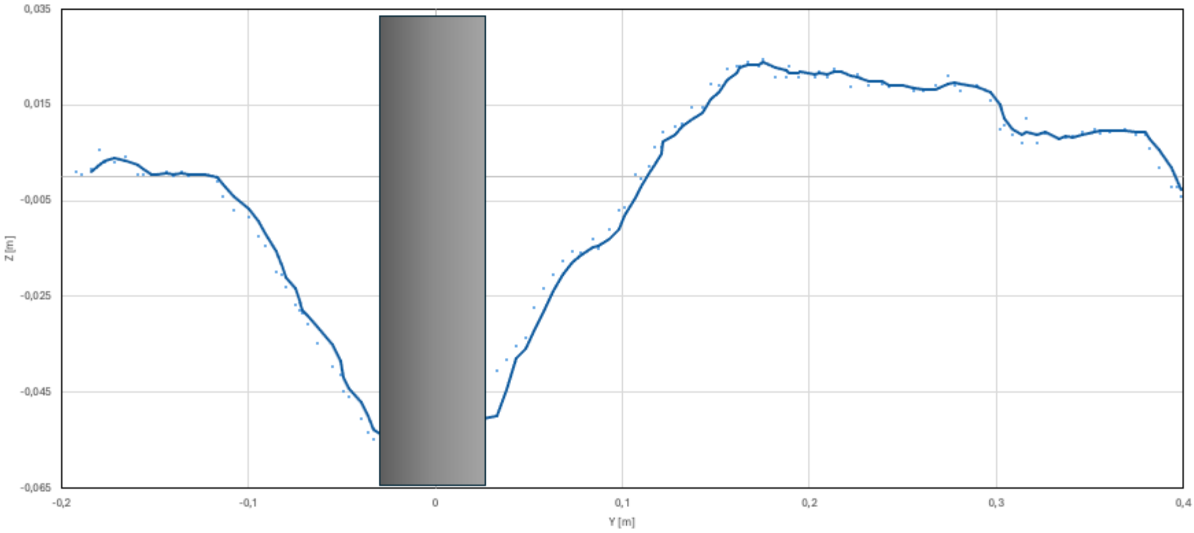

Figure A.3 3. Longitudinal profile for Fine Sand 1 over Fine Sand 2

A.4. FINE SAND 1 OVER COARSE SAND

Time(min)	S (cm)	S/D	Time (min)	S(cm)	S/D
0	0.0	0.00	**50**	3.6	0.72
1	1.5	0.30	**55**	3.7	0.74
2	1.6	0.32	**60**	3.9	0.78
3	2.0	0.40	**70**	3.9	0.78
4	2.2	0.44	**80**	3.9	0.78
5	2.3	0.46	**90**	4.0	0.80
6	2.4	0.48	**100**	4.0	0.80
7	2.6	0.52	**110**	4.1	0.82
8	2.6	0.52	**120**	4.1	0.82
9	2.7	0.54	**150**	4.2	0.84
10	2.7	0.54	**180**	4.2	0.84
11	2.8	0.56	**210**	4.3	0.86
12	2.9	0.58	**240**	4.4	0.88
13	2.9	0.58	**300**	4.5	0.90
14	3.0	0.60	**360**	4.5	0.90
15	3.1	0.62	**420**	4.6	0.92
20	3.3	0.66	**480**	4.7	0.94
25	3.4	0.68	**540**	4.8	0.96
30	3.5	0.70	**600**	4.9	0.98
35	3.6	0.72	**660**	5	1.00
40	3.6	0.72	**720**	5.1	1.02
45	3.6	0.72	**780**	5.1	1.02

Table A.4 1. Pile readings for Fine sand 1 over Coarse Sand

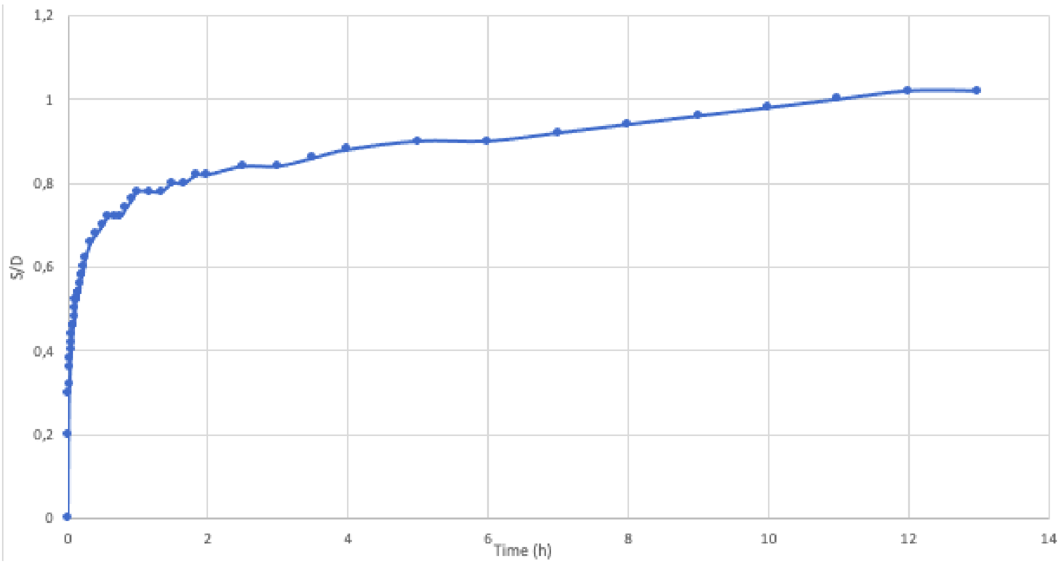

Figure A.4 1. Scour depth vs time for Fine Sand 1 over Coarse Sand

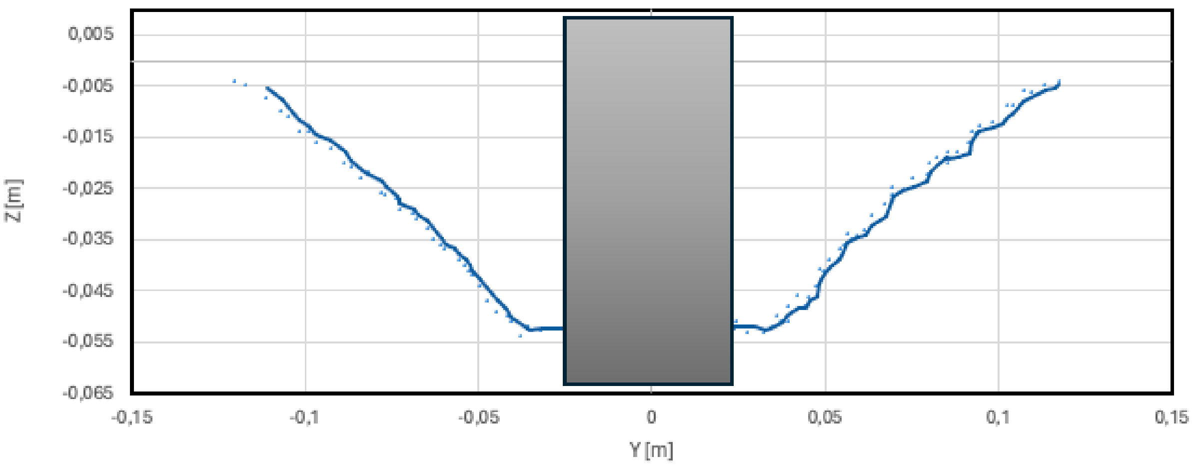

Figure A.4 2. Perpendicular profile for Fine Sand 1 over Coarse Sand

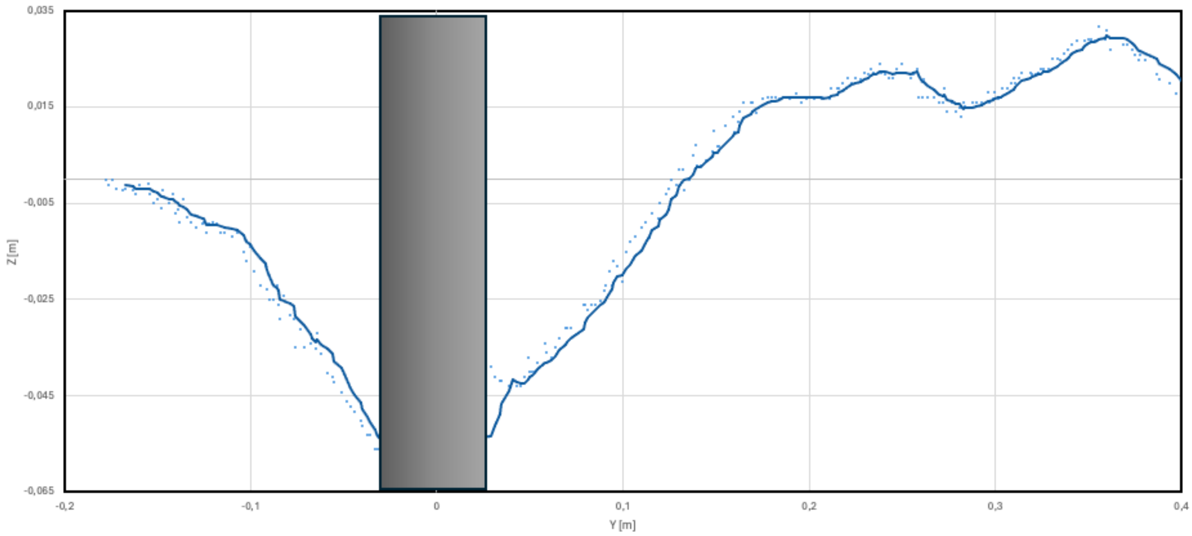

Figure A.4 3. Longitudinal profile for Fine Sand 1 over Coarse Sand

A.5. COARSE SAND OVER FINE SAND 1

Time(min)	S (cm)	S/D	Time (min)	S(cm)	S/D
0	0	**0**	**50**	3.1	0.62
1	1.3	**0.26**	**55**	3.3	0.66
2	1.5	**0.30**	**60**	3.5	0.70
3	1.6	**0.32**	**70**	3.8	0.76
4	1.7	**0.34**	**80**	3.9	0.78
5	1.7	**0.34**	**90**	4	0.80
6	1.7	**0.34**	**100**	4.1	0.82
7	1.8	**0.36**	**110**	4.1	0.82
8	1.8	**0.36**	**120**	4.1	0.82
9	1.8	**0.36**	**150**	4.2	0.84
10	1.8	**0.36**	**180**	4.4	0.88
11	2.0	**0.40**	**210**	4.4	0.88
12	2.0	**0.40**	**240**	4.5	0.90
13	2.1	**0.42**	**300**	4.5	0.90
14	2.3	**0.46**	**360**	4.5	0.90
15	2.4	**0.48**	**420**	4.5	0.90
20	2.5	**0.50**	**480**	4.5	0.90
25	2.7	**0.54**	**540**	4.5	0.90
30	2.8	**0.56**	**600**	4.5	0.90
35	2.9	**0.58**	**660**	4.5	0.90
40	2.9	**0.58**	**720**	4.5	0.90
45	3	**0.60**	**780**	4.5	0.90

Table A.5. 1. Pile readings for Coarse Sand over Fine Sand 1

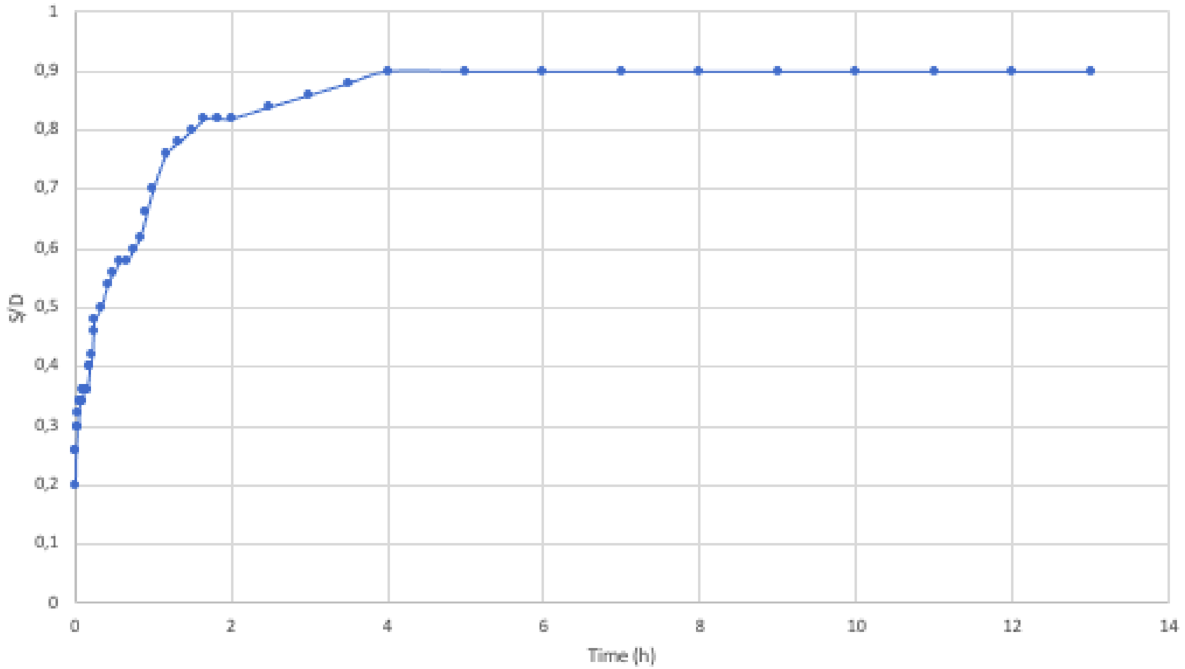

Figure A.5. 1. Scour depth vs time for Coarse Sand over Fine Sand 1

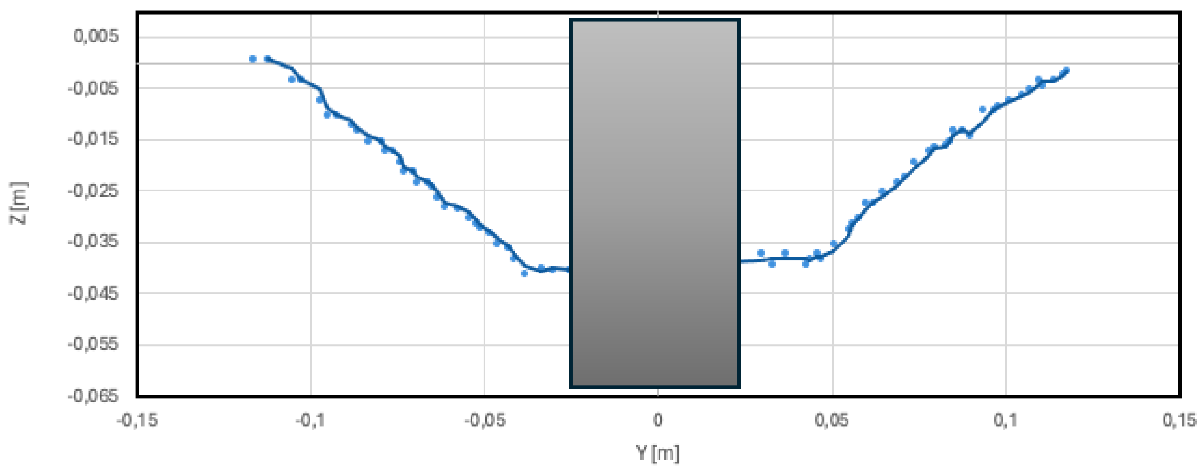

Figure A.5. 2. Perpendicular profile for Coarse Sand over Fine Sand 1 test

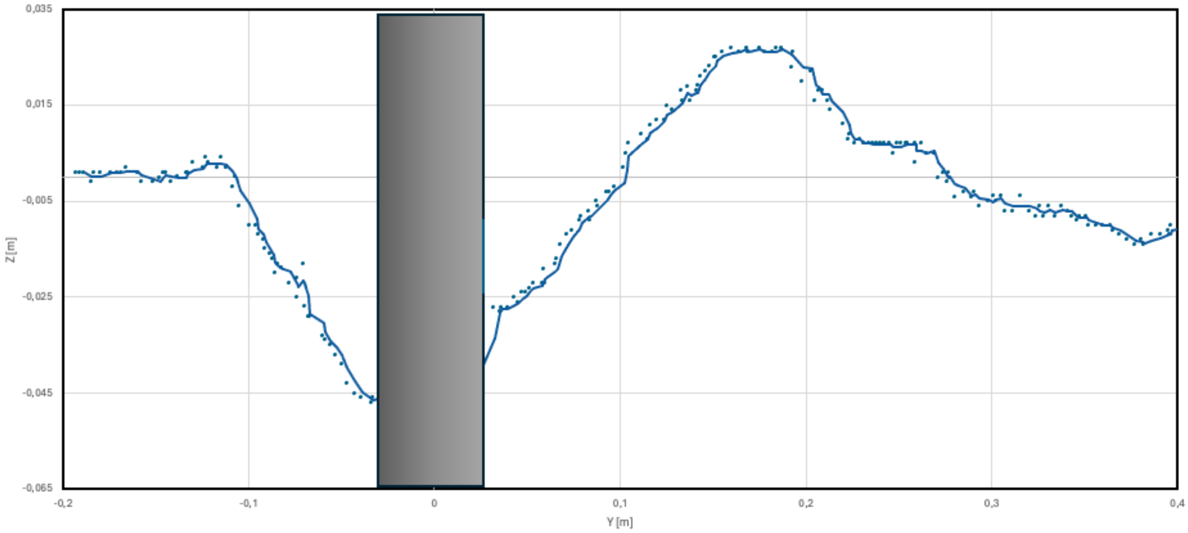

Figure A.5. 3. Longitudinal profile for Coarse Sand over Fine Sand 1 test